Research on Engineering Structures & Materials
www.jresm.org
MIM Research Group

Research Article

Analytical predictive modeling of the mechanical and thermal characteristics of concrete walls altered by pumice powder

Kahlouche Ramdane [*,1,a], Benfrid Abdelmoutalib [2,3,b], Ferkous Saci Abdelhakim [4,c], Yahi Takai Eddine [5,6,d]

[1]*Dept. of Public Works, Mouloud Mammeri University, 15000 Tizi Ouzou, Algeria*
[2]*Dept. of Civil Eng. & Public Works, Djillali Liabes University, 22000 Sidi Bel Abbes, Algeria*
[3]*Libyan Society for Research and Scientific Studies, Libya*
[4]*Dept. of Civil Eng., Faculty of Technology, University M'hamed Bougera, 35000 Boumerdes, Algeria*
[5]*Dept. of Hydraulic, Mouloud Mammeri University, Tizi-Ouzou, 15000, Algeria*
[6]*Laboratory of Geomaterials, Environment and Development, Mouloud Mammeri University, Tizi-Ouzou, 15000, Algeria*

Article Info

Article History:

Received 14 Dec 2025

Accepted 08 Mar 2026

Keywords:

Pumice powder;
Eco-concrete;
Analytical modeling;
Thermo-mechanical behavior;
Maxwell–Eucken model;
Thermal conductivity

Abstract

The transition toward energy-efficient buildings requires integrated thermo-mechanical design rather than purely structural assessment. Construction materials must simultaneously govern stiffness, thermal expansion, and heat transfer without compromising stability. Partial cement replacement enables tailored performance. Pumice powder (PP), rich in amorphous silica, undergoes pozzolanic reactions that refine the concrete microstructure, influencing both mechanical stiffness and thermal conductivity; however, a unified analytical framework quantifying its coupled thermo-mechanical response at the structural level remains lacking. To address this, an analytical framework is developed to evaluate the influence of PP on effective thermo-elastic properties. Homogenized elastic properties are derived using a two-phase model, while thermal parameters are calculated with the Maxwell–Eucken approach. Both sets of properties are incorporated into a refined High-Order Deformation plate Theory (RPT) to determine the critical mechanical buckling load and the critical thermal buckling temperature of structural walls. Predictions are validated against independent experimental data from the literature. At 10% PP replacement, the elastic modulus decreases by approximately 18%, accompanied by a 19% reduction in the critical mechanical buckling load. In contrast, thermal performance improves: the thermal resistance increases by about 18–20%, while the thermal transmittance and heat flux decrease by approximately 17%. Additionally, the critical thermal buckling load increases by nearly 16%. These results quantify the trade-off between reduced stiffness and enhanced thermal stability, demonstrating how PP incorporation modifies the mechanical and thermal instability thresholds of concrete walls.

1. Introduction

Concrete technology is undergoing a significant transformation driven by the twin imperatives of sustainable construction and mitigating global climate change. The Intergovernmental Panel on Climate Change (IPCC) emphasizes that urgent transitions in industrial sectors are required to limit global warming to 1.5°C, directly implicating the construction industry [1]. Portland cement production alone contributes approximately 7–8% of global CO_2 emissions, while the broader

*Corresponding author: ramdane.kahlouche@ummto.dz
[a]orcid.org/0000-0002-3288-2939; [b]orcid.org/0009-0007-8171-1654; [c]orcid.org/0009-0001-6561-5044; [d]orcid.org/0009-0008-7133-8224
DOI: http://dx.doi.org/10.17515/resm2026-1404me1214rs

construction sector accounts for nearly 36% of global energy consumption and 30% of anthropogenic greenhouse gas emissions [2-4]. These challenges are closely aligned with the United Nations Sustainable Development Goals (SDGs), particularly SDG 9 (Industry, Innovation, and Infrastructure) and SDG 13 (Climate Action), which promote resource-use efficiency and the adoption of environmentally sound technologies [5].

In response, the Global Cement and Concrete Association (GCCA) has pledged a 25% reduction in CO_2 emissions by 2030, as a key step toward achieving "Net Zero" concrete by 2050 [6]. This roadmap focuses on reducing clinker intensity, optimizing concrete mix designs, and accelerating the use of low-carbon supplementary materials, which account for nearly 60% of global cement and concrete demand (Fig. 1). These environmental imperatives have driven research into alternative binders and supplementary cementitious materials (SCMs), such as volcanic pozzolans and lightweight aggregates, which can reduce the carbon footprint while improving thermal performance and maintaining structural integrity [7, 8]. Partial replacement of cement with natural pozzolanic additives has demonstrated technical feasibility and notable environmental benefits [9-12]. In addition, micro- and nanoscale reinforcements have shown potential to enhance stiffness, thermal behavior, and long-term durability, enabling the design of energy-efficient concrete structures that meet both mechanical and thermal performance requirements under variable service conditions [13-18].

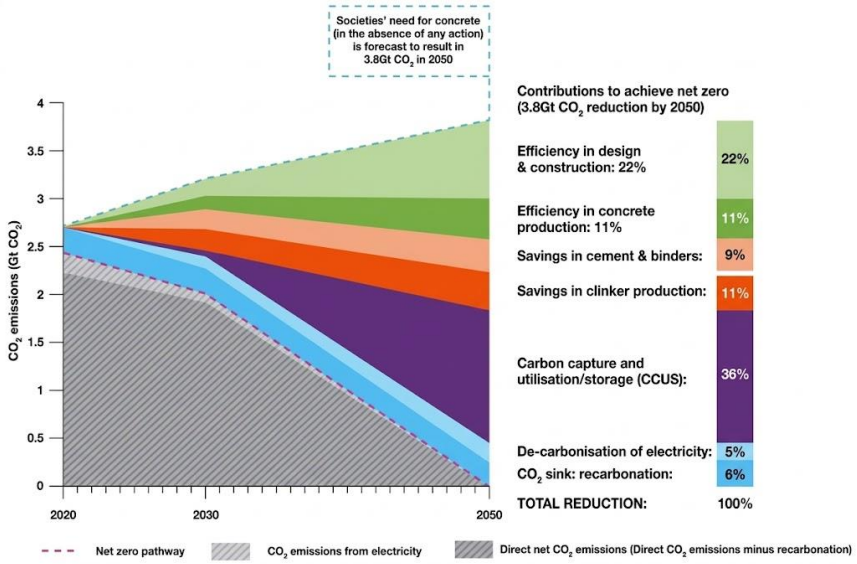

Fig. 1. Roadmap to Net Zero: Projected CO_2 emissions reduction targets for the global cement and concrete sector (2020–2050) [6]

While many supplementary cementitious materials (SCMs) primarily enhance concrete through chemical reactivity, pumice powder (PP) is distinguished by its porous cellular structure and inherent pozzolanic activity, which simultaneously reduce concrete weight and improve thermal performance. These unique characteristics make PP particularly suitable for exploring how microstructural modifications influence both material-level properties and overall structural behavior. As a result, recent studies have highlighted that PP, which can range from nanometric to macroscopic particle sizes, can substantially influence the mechanical and thermal properties of concrete, highlighting its potential as a multi-scale reinforcement for high-performance eco-concretes. This multi-scale behavior is conceptually similar to other studies that have explored nanoscale and microscale additives, where homogenization and multi-phase modeling approaches were employed to capture particle-matrix interactions and predict enhanced stiffness, thermal conductivity, and buckling resistance. For example, Harrat et al. [19] utilized the Voigt homogenization model to examine nano-silica-reinforced concrete beams, demonstrating significant enhancements in stiffness and load-bearing capacity. Chatbi et al. [20] advanced this methodology by utilizing a sophisticated two-dimensional Voigt framework for concrete slabs, emphasizing the necessity of precisely capturing planar stress distributions to effectively predict deflections. Complementary studies have utilized the Eshelby tensor to examine particle-matrix

interactions in heterogeneous composites, such as glass powder- or metal oxide-reinforced panels, demonstrating that nanoscale inclusions can substantially alter both elastic moduli and thermal expansion coefficients. Dine El Hannani et al. [21] emphasized the impact of nanoparticle type and concentration on buckling resistance and free vibration properties, whereas Kecir et al. [22] and Harrat et al. [23, 24] validated that iron nanoparticle reinforcement improves flexural rigidity under thermo-mechanical stress. Recent studies have expanded homogenization models to encompass natural and engineered microscale additives, such as wheat straw and recycled glass, utilizing Liwes, Nielsen Spar, and Maxwell–Eucken formulations to forecast integrated mechanical–thermal responses [25]. These investigations collectively demonstrate the critical role of multiscale modeling in engineering concrete with tailored stiffness and thermal conductivity properties, thereby providing a methodological framework for the application of pumice powder as an environmentally sustainable pozzolanic additive.

While nanoscale reinforcements provide targeted performance improvements, geological additives remain highly attractive due to their cost-effectiveness, sustainability, and multi-functional benefits. Among these, pumice powder (PP) has been shown to improve mechanical and thermal characteristics of concrete through both aggregate replacement and partial cement substitution. Cavaleri et al. [26] experimentally demonstrated that PP aggregates can reduce concrete density while maintaining structural integrity. Granata [27] highlighted that the pozzolanic reactivity of PP decreases voids and enhances strength in self-compacting concretes. Kurt et al. [28] reported that PP improves thermal insulation and reduces weight, although excessive content can negatively affect segregation and hydration kinetics. Zeyad et al. [29-31] further investigated volcanic pumice dust in geopolymer and high-strength concretes, showing enhancements in compressive and flexural strengths, reduction in water absorption and porosity, and benefits under self-curing and hot-weather conditions. Hossain [32] demonstrated that volcanic PP can produce blended cements with extended setting times, low heat of hydration, and mechanical performance comparable to fly ash cement for up to 20% replacement. Karthika et al. [33] confirmed that partially replacing coarse aggregates with PP at 50–100% reduces self-weight, decreases dead load, and improves thermal insulation, while maintaining favorable mechanical and durability performance. A comprehensive review by Moolchandani [34] synthesized over 60 studies, emphasizing that PP's high amorphous silica content and porous morphology provide intrinsic pozzolanic reactivity, internal curing potential, and long-term durability. The review also quantified late-age compressive strength gains of 6–11%, reduced chloride permeability by 22–35%, improved sulfate resistance by up to 28%, and demonstrated significant reductions in thermal conductivity (30–56%) and surface temperatures (up to 42%) when combined with phase-change materials. Ghanim et al. [35] confirmed that textile-industry-derived PP possesses higher pozzolanic potential than fly ash, improving early-age workability and mechanical properties, with 25% replacement identified as optimal. Collectively, these studies demonstrate that PP's chemical reactivity, porous microstructure, and internal curing capacity simultaneously enhance mechanical performance, durability, and thermal efficiency, making it a highly suitable additive for sustainable, energy-efficient concrete walls.

To elucidate the enhancements in mechanical, thermal, and durability properties observed in PP-modified concrete, it is crucial to examine the underlying chemical and microstructural mechanisms. The pozzolanic activity of pumice powder (PP) is primarily driven by its high content of amorphous silica (SiO_2) and alumina (Al_2O_3). The SiO_2 reacts with calcium hydroxide ($Ca(OH)_2$) during cement hydration to form additional calcium silicate hydrate (C-S-H) gel, which is the main contributor to mechanical strength and microstructural densification [36, 37]. Simultaneously, Al_2O_3 interacts with available calcium and sulfate ions to promote the formation of calcium aluminosilicate hydrates (C-A-S-H) and ettringite [38]. These secondary hydration products effectively fill the micro-voids within the interfacial transition zone (ITZ), the typically porous and mechanically weaker region between the cement paste and pumice aggregates [39]. By refining the ITZ, the Al_2O_3-driven reactions enhance stress transfer across the composite phases, mitigating the strength reduction often associated with lightweight aggregates [40]. From a thermal perspective, the densified ITZ decreases the presence of large interconnected pores at the particle-matrix interface. Although this slightly increases localized solid-to-solid contact, the combination of a high

silica-to-calcium ratio and the intrinsic cellular porosity of pumice remains the dominant factor in lowering the effective thermal conductivity of the concrete [41, 42].

The chemical composition of pumice, as summarized in Table 1, includes minor oxides such as Fe_2O_3, Na_2O, and K_2O, which can influence setting time, workability, and thermal behavior. These compositional characteristics, together with the pozzolanic activity of SiO_2 and Al_2O_3, support the use of PP as both a partial cement replacement and a lightweight aggregate, enabling concrete walls with optimized mechanical and thermal performance.

Table 1. Chemical composition (wt%) of different pumice specimens reported in literature.

Composition	Ref	SiO_2	Al_2O_3	Na_2O	K_2O	Fe_2O_3	CaO	MgO	P_2O_5
Pumice specimen 1	Xiyu et al. [43]	72.06	9.39	4.29	4.04	3.40	0.25	0.02	0.002
Pumice specimen 2	Shi et al. [44]	68.64	11.92	5.53	4.93	3.45	0.73	0.10	0.06
Pumice specimen 3	Turhan et al. [45]	75.51	9.94	2.04	5.12	1.10	0.25	0.04	<0.001

Physically, the performance of pumice powder and pumice-based aggregates is strongly influenced by the highly porous and vesicular morphology of the material. As illustrated in Fig. 2, the SEM micrographs reveal a multi-scale network of interconnected voids and thin-walled cavities, which act as natural reservoirs for internal curing water. This intrinsic porosity enables gradual moisture release during hydration, mitigating autogenous shrinkage and promoting continuous formation of hydration products. The low density of pumice further contributes to reducing the self-weight of concrete elements while enhancing thermal insulation due to the presence of air-filled pores. Additionally, the irregular surface texture improves mechanical interlocking within the interfacial transition zone (ITZ), resulting in better stress transfer under mechanical loading and more uniform thermal diffusion. Combined, these physical features provide a mechanistic explanation for the reductions in thermal conductivity, enhanced durability, and improved long-term mechanical performance observed in PP-modified concrete [43].

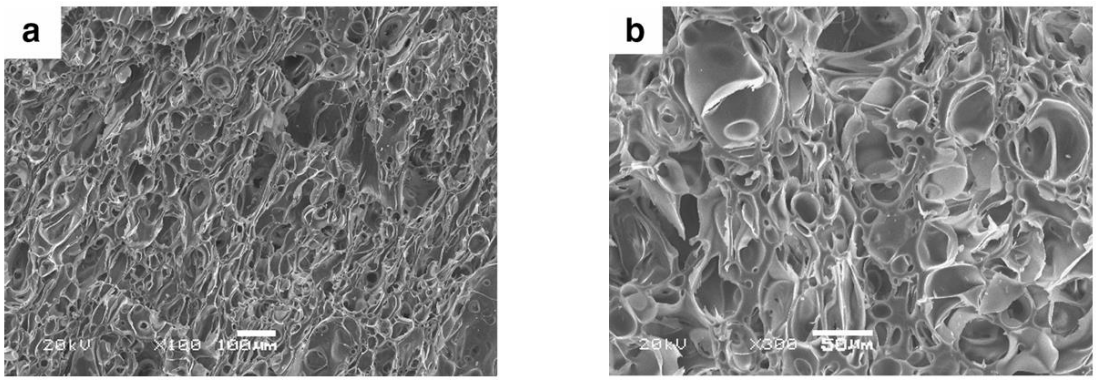

Fig. 2. Scanning electron microscopy (SEM) images showing the morphology of pumice at magnifications of : (a) 100× and (b) 300×[43]

To consolidate the insights obtained from recent works on the use of pumice powder (PP) in cementitious systems, Table 2 presents a structured synthesis of the main physical, chemical, and thermal effects reported in the literature. As shown in the table, PP influences concrete behavior on several interconnected levels: it alters density and porosity, affects fresh and hardened properties, contributes to hydration kinetics and pozzolanic reactions, and promotes microstructural refinement through the formation of additional C–S–H. These transformations also translate into improved thermal performance, particularly in terms of heat moderation, insulation capacity, and resistance to temperature-induced degradation. By gathering these findings into a single framework, Table 2 provides a clear understanding of how PP contributes to performance enhancement across multiple scales, thereby reinforcing its relevance as a sustainable supplementary cementitious material. This consolidated evidence forms the basis for the present study, which aims to analytically examine the coupled mechanical and thermal response of concrete walls incorporating PP.

Table 2. Summary of physical, chemical, and thermal effects of pumice powder (PP) in cementitious materials and concrete as reported in recent studies

Ref	PP Type	Physical Effects	Chemical Effects / Pozzolanic Activity	Thermal / Microstructural Influence
[46]	Saturated PP, 0.6–1.25 mm, partial sand replacement	Reduced persistent shrinkage, internal curing effect	Accelerated early hydration, promoted secondary hydration of active mineral admixtures; modified C-S-H composition (Ca/Si ratio)	Enhanced microstructure in local effective area; improved temperature stability via denser hydration products
[47]	PP blended cement, up to 30% cement replacement	Shorter setting time despite lower clinker, lower workability	Pozzolanic reaction contributes to compressive strength, chemical composition correlates with strength	Minor thermal effect noted; influence on hydration heat not detailed
[48]	PP as cementitious material or lightweight aggregate	Reduced unit weight, improved thermal and acoustic insulation, decreased drying shrinkage, increased fire resistance	Pozzolanic activity decreases porosity, mitigates ASR expansion	Lower hydration heat, improved thermal stability, packed microstructure reduces permeability
[49]	PP as aggregate or cement substitute, 5–25%	Improved strength (especially 10–25% PP), lower water absorption, reduced porosity	Pozzolanic activity strongest at 28–90 days; enhances long-term durability	Packed pore structure, better heat transfer and thermal insulation in SCMs
[50]	PP, 25% replacement in geopolymer concrete	Decreased density, lower compressive strength at higher content	Pozzolanic reaction limited in high-porosity PP; contributes to durability via pore structure refinement	SEM shows denser microstructure in optimal mixes; thermal stability improved at moderate replacement
[51]	Ultrafine PP in HPC, binary/ternary mixes	Higher electrical resistivity, low permeability, enhanced long-term durability	Strong pozzolanic contribution, interacts with other SCMs to enhance compressive strength	Improved corrosion resistance under thermal stress; thermal insulation improved via dense microstructure
[52]	PP + polypropylene fibers, 10–40% cement replacement	Enhanced compressive and tensile strength, better ductility	Cementitious characteristics of PP; contributes to strength via pozzolanic activity	Microstructure densification improves thermal and mechanical performance
[36]	PP replacement 5–25%	Reduced density, delayed setting, decreased workability	$SiO_2 + Al_2O_3 + Fe_2O_3 > 70\%$; pozzolanic, enhances C-S-H formation	Improved microstructural cohesion; moderate thermal effect via lower hydration heat
[53]	PP, 3–18% cement replacement	Enhanced CS, FS, STS, and MOE up to 12%; decreased strength beyond	Pozzolanic reaction forms additional C-S-H; contributes to mechanical property improvement	Thermal stability improved indirectly via denser microstructure; validated via RSM optimization
[54]	PP, 15–50% cement replacement	Strength comparable to control up to 25%; density reduction	Pozzolanic constituents enhance C-S-H formation and durability	Microstructure improved; XRD confirms mineral phases conducive to long-term stability

The data compiled in Table 2 demonstrate that pumice powder influences concrete at multiple levels, including physical, chemical, and thermal aspects. PP alters density, porosity, and shrinkage

behavior while contributing to hydration kinetics and pozzolanic reactions that enhance microstructural cohesion and long-term durability. Thermal performance is also affected, with improvements in insulation, heat transfer, and stability under temperature variations. However, the magnitude and timing of these effects vary widely depending on PP type, replacement ratio, particle size, and concrete mix, making it challenging to generalize or predict wall-level behavior from individual experimental results. This variability highlights a critical need for an analytical framework capable of systematically linking PP content, effective thermo-mechanical properties, and structural response. Such a framework would allow prediction of mechanical stiffness, thermal response, and instability thresholds of PP-modified concrete walls, bridging the gap between material-level observations and design-scale applications.

At the structural level, translating these material-level trends into reliable predictions of wall behavior further requires an appropriate mechanical modeling framework. Given the multi-scale effects induced by PP, ranging from microstructural densification to modifications in thermal transport, predicting the thermo-mechanical response of concrete walls demands analytical models capable of capturing bending, shear, and temperature-driven gradients with greater fidelity than classical formulations. Because PP alters density, stiffness, porosity, and thermal conductivity, the resulting wall behaves as a heterogeneous and thermally sensitive system, rendering classical plate assumptions inadequate. Classical plate theory (Kirchhoff–Love), which neglects transverse shear deformation, often fails to represent the behavior of moderately thick structural elements, especially when temperature gradients induce significant through thickness stresses [55]. These shortcomings have motivated the development of refined plate and shell theories. First order shear deformation theory (FSDT), introduced by Mindlin and Reissner, enhances realism by incorporating shear deformation; however, it relies on shear correction factors that introduce uncertainty when applied to materials whose internal structure has been modified by lightweight pozzolanic inclusions such as PP [56]. To overcome these limitations, higher order shear deformation theories (HSDT), as developed by Reddy [57], Touratier [58], and Karama [59], provide more accurate displacement fields by naturally capturing the parabolic distribution of shear strains without correction factors, making them particularly suitable for non-homogeneous cementitious composites.

The effectiveness of these refined theories is well demonstrated in the literature for functionally graded, layered, and thermally responsive materials, which share notable similarities with PP blended concrete. For instance, Lee et al. [60] studied thermoelastic bending of plates with temperature dependent properties, while Sun et al. [61] examined thermal buckling in heterogeneous plates, emphasizing the strong role of thermal loading in stability behavior. Prakash and Ganapathi [62] further highlighted the influence of coupled thermal mechanical effects on vibration responses. More recent contributions by Zenkour [63], Yang et al. [64], Niknam and Akbarzadeh [65] and Mallios et al. [66] confirmed the superior predictive capacity of HSDT and FEM formulations for plates with spatially varying stiffness and conductivity, conditions directly representative of PP modified concrete. Additionally, Sayyad and Ghugal [67-71] demonstrated that refined trigonometric theories provide high accuracy for thick concrete like plates, especially under non uniform thermal fields.

Building on the observed material-level effects of PP, the present work proposes a comprehensive analytical framework that systematically links PP incorporation to both material and structural performance of concrete walls. The study first evaluates the influence of PP content (2.5–10 wt%) on the effective elastic properties, including Young's modulus, and thermal behavior, including expansion coefficient and thermal conductivity, establishing quantitative relationships for PP-modified concrete as a construction material. These homogenized properties are then incorporated into a refined High-Order Deformation Plate Theory (RPT) to simulate wall behavior under mechanical and thermal loads. Mechanical stability is analyzed through uniaxial and biaxial critical buckling loads, considering variations in wall slenderness (length-to-thickness ratio). Thermal effects are further incorporated by evaluating temperature distributions across the wall, enabling calculation of the thermal critical buckling temperature. In addition, thermal performance indicators, including thermal resistance (R), thermal transmittance (U), and heat flux (ϕ), are quantified for walls of varying thickness and PP content. By simultaneously addressing elastic,

thermal, and stability characteristics, this framework provides a unified predictive tool to assess how PP modifies both material behavior and structural response, offering a basis for optimized wall design in energy-efficient and mechanically reliable constructions.

2. Analytical Framework for Evaluating Thermo-Mechanical Properties of PP-Modified Concrete Walls

The analytical formulation of the pumice powder (PP)-modified concrete wall is established based on the kinematic and constitutive assumptions defined within the proposed homogenization framework. The study considers a simply supported wall of dimensions $a \times b \times h_w$, incorporating PP inclusions to assess their influence on the coupled thermo-mechanical response. A refined plate deformation theory is employed to capture shear deformation effects and through-thickness temperature variations accurately.

The geometrical configuration of the PP-modified concrete wall is illustrated in Fig. 3, defined by its length (a), width (b), and thickness (h_w). The wall is modeled as a rectangular plate with all edges simply supported. This boundary condition is selected because it provides a mechanically conservative and analytically tractable configuration that is widely adopted in stability analyses of wall and slab systems. In practice, many load-bearing and infill walls exhibit rotational restraint with limited moment continuity at supports, making the simply supported assumption a rational idealization for evaluating critical buckling behavior while avoiding overestimation of structural stiffness.

Thermal loading is applied through a temperature gradient across the thickness, representing heat transfer from the exterior environment toward the interior space (see Fig. 3), consistent with building envelope conditions under solar exposure or seasonal temperature variations. This through-thickness thermal distribution induces in-plane thermal stresses due to restrained expansion, which may contribute to thermal buckling instability.

2.1. Kinematical Formulation of the PP-Modified Concrete Slab

Assuming small deformations and linear thermo-elastic behavior, the total strain field of the PP-modified concrete wall is represented as the superposition of mechanical and thermal components. The constitutive relationships are formulated using the homogenized elastic moduli and the effective coefficients of thermal expansion derived from the two-phase homogenization scheme. In accordance with the refined plate theory, the displacement components along the x, y, and z directions (U, V, and W, respectively) are expressed as functions of the mid-plane displacements and higher-order shear deformation terms, as follows [72]:

$$U(x,y,z) = u_0(x,y) - z\frac{\partial w_b(x,y)}{\partial x} + f(z)\frac{\partial w_s(x,y)}{\partial x} \tag{1.a}$$

$$V(x,y,z) = v_0(x,y) - z\frac{\partial w_b(x,y)}{\partial y} + f(z)\frac{\partial w_s(x,y)}{\partial y} \tag{1.b}$$

$$W(x,y,z) = w_b(x,y) + w_s(x,y) \tag{1.c}$$

The in-plane displacements of a point located on the mid-surface of the PP-modified concrete wall are denoted by $u_0(x,y)$ and $v_0(x,y)$ along the x and y directions, respectively, and represent the membrane deformation of the wall associated with in-plane stretching and compression under mechanical and thermal loads. The transverse displacement $w(x,y,z)$ is decomposed into two physically distinct components: $w_b(x,y)$, which represents the bending-induced displacement governing the global flexural response and buckling instability of the wall, and $w_s(x,y)$, which represents the transverse shear deformation associated with non-uniform through-thickness strain. The bending component w_b primarily controls the wall's response to in-plane mechanical loads and thermally induced membrane stresses, and therefore directly influences the critical mechanical and thermal buckling conditions. In contrast, the shear component w_s accounts for transverse shear flexibility, which becomes significant in moderately thick walls and in PP-modified concrete due to reduced stiffness and material heterogeneity. This component affects stress redistribution, deformation localization, and the overall stiffness of the wall, thereby

modifying the thermo-mechanical stability response, particularly under combined mechanical loading and temperature gradients. The thickness coordinate z is measured from the mid-plane, in which:

$$x \in (0,a); y \in (0,b); z \in (-h_w/2\,; h_w/2) \tag{2}$$

In this study, the higher-order shear deformation theory (HSDT) proposed by Mourad Chitour et al. [73] is adopted to accurately capture the nonlinear distribution of transverse shear strains across the slab's thickness without the need for a shear correction factor. Compared to classical plate theory, which neglects transverse shear, and first-order shear deformation theory (FSDT), which requires shear correction factors and may introduce inaccuracies for moderately thick or heterogeneous materials, HSDT provides a more realistic representation of shear effects in PP-modified concrete walls. The employed shape function $f(z)$ defines the variation of shear deformation through the slab's thickness and is expressed as:

$$f(z) = \frac{3}{35}\pi z\left(\pi - \sqrt[3]{0.135}\,cosh\left(\frac{\pi z}{h}\right)\right); \quad g(z) = \frac{df(z)}{dz} \tag{3}$$

The constitutive stress–strain relationships governing the thermo-elastic response of the PP-modified concrete wall are formulated by incorporating both mechanical and thermal effects. The material is assumed to behave as a linear, homogeneous, and isotropic continuum characterized by the effective (homogenized) elastic constants obtained from the two-phase model.

$$\varepsilon_y = \frac{\partial V(x,y,z)}{\partial y} = \frac{\partial v_0}{\partial y} - z\frac{\partial^2 w_b}{\partial y^2} - f(z)\frac{\partial^2 w_s}{\partial y^2} \tag{4.a}$$

$$\gamma_{xy} = \frac{\partial U(x,y,z)}{\partial y} + \frac{\partial V(x,y,z)}{\partial x} = \left(\frac{\partial v_0}{\partial x} + \frac{\partial u_0}{\partial y}\right) - 2z\frac{\partial^2 w_b}{\partial x \partial y} - 2f(z)\frac{\partial^2 w_s}{\partial x \partial y} \tag{4.b}$$

$$\gamma_{xz} = \frac{\partial U(x,y,z)}{\partial z} + \frac{\partial W(x,y,z)}{\partial x} = \left(1 - \frac{df(z)}{dz}\right)\frac{\partial w_s}{\partial x} \tag{4.c}$$

$$\gamma_{yz} = \frac{\partial V(x,y,z)}{\partial z} + \frac{\partial W(x,y,z)}{\partial y} = \left(1 - \frac{df(z)}{dz}\right)\frac{\partial w_s}{\partial y} \tag{4.d}$$

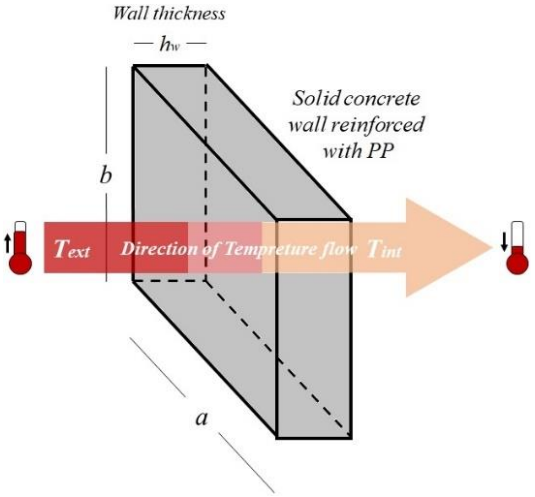

Fig. 3. Geometrical configuration of the PP-modified concrete slab, showing its dimensions (a, b, h_w) and the direction of heat transfer from the external surface (T_{ext}) toward the internal surface (T_{int})

Accordingly, the total stress components are expressed as functions of the mechanical strain and the temperature-induced strain resulting from uniform or gradient temperature fields. The generalized constitutive relations can thus be written as:

$$\begin{Bmatrix}\sigma_x\\ \sigma_y\\ \tau_{xy}\\ \tau_{xz}\\ \tau_{yz}\end{Bmatrix}=\begin{bmatrix}\tilde{Q}_{11} & \tilde{Q}_{12} & 0 & 0 & 0\\ \tilde{Q}_{12} & \tilde{Q}_{22} & 0 & 0 & 0\\ 0 & 0 & \tilde{Q}_{66} & 0 & 0\\ 0 & 0 & 0 & \tilde{Q}_{44} & 0\\ 0 & 0 & 0 & 0 & \tilde{Q}_{55}\end{bmatrix}\begin{Bmatrix}\varepsilon_x-\alpha_{hom}T\\ \varepsilon_y-\alpha_{hom}T\\ \gamma_{xy}\\ \gamma_{xz}\\ \gamma_{yz}\end{Bmatrix} \quad (5)$$

Here, $\tilde{Q}_{ij}$ denotes the reduced elastic constants of the homogenized PP-modified concrete system, which is treated as isotropic. These constants account for the combined contribution of the concrete matrix and the PP reinforcement and are obtained using the adapted Reuss–Voigt–Luo homogenization model, where:

$$\tilde{Q}_{11}=\tilde{Q}_{22}=\frac{(1-\upsilon_{hom})E_{hom}}{(1+\upsilon_{hom})(1-2\upsilon_{hom})};\ \tilde{Q}_{12}=\frac{\upsilon E_{hom}}{(1+\upsilon_{hom})(1-2\upsilon_{hom})}$$
$$\tilde{Q}_{66}=\tilde{Q}_{55}=\tilde{Q}_{44}=\frac{E_{hom}}{(1+\upsilon_{hom})} \quad (6)$$

2.2. Analytical Homogenization of PP-Modified Concrete

To determine the effective thermo-elastic properties (E_{hom}, υ_{hom}, α_{hom}, λ_{hom}) of the PP-modified concrete matrix, a two-phase homogenization approach based on the Voigt–Reuss–Luo model is adopted, accounting for three-dimensional stress interactions and Poisson's ratio coupling effects. The selection of a two-phase formulation is justified by the material configuration of PP-modified concrete, which consists of a dominant continuous cementitious matrix and dispersed pumice particles acting as inclusions. Within the investigated replacement range (0%–10%), PP remains sufficiently distributed to be reasonably idealized as a secondary phase embedded in a continuous matrix, without forming a percolating or interconnected skeleton. This assumption enables analytical tractability while preserving the essential mechanical and thermal interaction mechanisms between phases. The homogenization procedure is carried out in two successive phases [74, 75]:

- Phase I: Homogeneous Concrete Matrix

Initially, the concrete is assumed to be homogeneous and isotropic, representing a mono-phasic state corresponding to conventional unreinforced concrete. This baseline serves as a reference for evaluating the impact of PP inclusion on the mechanical and thermal behavior of the composite wall. The material properties of the concrete matrix are characterized by the elastic modulus (E_c), Poisson's ratio (ν_c), thermal conductivity (λ_c), and coefficient of thermal expansion (α_c).

- Phase II: Bi-Phasic Composite Material

With the incorporation of PP as a partial replacement for cement or fine aggregate, the mixture transforms into a bi-phasic composite, composed of the continuous concrete matrix and dispersed PP inclusions. The volumetric fraction of PP (υ_{PP}) ranges from 0% (pure concrete) to 10%, enabling a systematic assessment of its influence on the wall's mechanical stiffness, thermal expansion, and heat transfer performance. The two homogenization phases and the underlying assumptions are conceptually illustrated in Fig. 4, which shows the transition from mono-phasic concrete to bi-phasic PP-reinforced concrete and the assumed spherical distribution of PP inclusions within the matrix.

- Porous Spherical Inclusions

PP particles are idealized as spherical or quasi-spherical inclusions with uniform internal porosity, representing their vesicular volcanic structure. Although natural pumice particles exhibit irregular shapes, microscopic observations reported in the literature indicate that crushed and ground pumice tends to form approximately equiaxed particles with rounded edges due to mechanical processing [76-78]. To accurately represent the behavior of the PP-reinforced composite, certain physical considerations are adopted within the homogenization framework.

In analytical homogenization theory, the spherical inclusion assumption is widely adopted because it provides a physically representative average geometry while allowing closed-form solutions for stress and heat transfer fields. Therefore, this idealization offers a rational balance between

microstructural realism and analytical tractability, without significantly affecting the prediction of effective elastic and thermal properties at moderate inclusion contents.

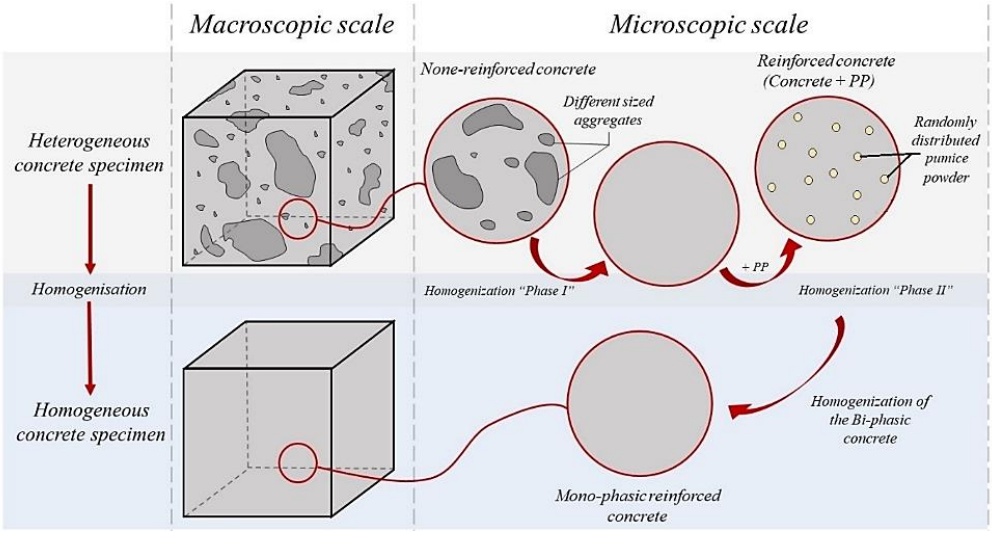

Fig. 4. Illustrates the conceptual homogenization, showing the transition from mono-phasic concrete to bi-phasic PP-reinforced concrete and the assumed distribution of spherical PP inclusions within the matrix

- Random Dispersion

PP inclusions are assumed to be randomly dispersed and non-agglomerated within the continuous cementitious matrix. This assumption is consistent with the requirements of classical homogenization theory, which relies on a statistically homogeneous representative volume element (RVE) where no preferential clustering or directional bias dominates the macroscopic response [79-81]. Within the investigated replacement range (≤10%), the inclusion phase remains discontinuous and well below typical percolation thresholds; consequently, inclusion–inclusion interactions are limited, and large-scale agglomeration effects are unlikely to govern the composite behavior [82]. Under these conditions, the mechanical stiffness and heat transfer characteristics are controlled primarily by matrix–inclusion interactions rather than localized particle clusters. Therefore, neglecting agglomeration provides a reasonable approximation for predicting effective averaged thermo-elastic properties at the structural scale [83].

2.2.1 Modelling Procedure Elasto-Mechanical Homogenization Using the Reuss–Voigt–Luo Model

The effective elastic properties of the PP-reinforced concrete are computed using an adapted Reuss–Voigt–Luo homogenization model, accounting for Poisson's ratio and three-dimensional stress interactions. The effective Young's moduli in the x, y, and z directions (E_{hom}^{x}, E_{hom}^{y}, E_{hom}^{z}) are expressed as [84]:

$$E_{hom}^{x} = E_{hom}^{y} = \frac{\{V_c(1+\upsilon_{pp})E_c + V_{pp}(1+\upsilon_c)E_{pp}\}\{V_c(1-\upsilon_{pp})E_c + V_{pp}(1-\upsilon_c)E_{pp}\}}{\{V_c(1-\upsilon_{pp}{}^2)E_c + V_{pp}(1-\upsilon_c{}^2)E_{pp}\}}$$

$$E_{hom}^{z} = \frac{E_c E_{pp}[V_c(1-\upsilon_{pp})E_c + V_{pp}(1-\upsilon_c)E_{pp}]}{\left\{\begin{matrix} E_c E_{pp}[V_c^2(1-\upsilon_{pp}) + V_{pp}^2(1-\upsilon_c)] \\ +\upsilon_{pp}\upsilon_c[(1+\upsilon_{pp})(1-2\upsilon_{pp})E_c^2 \\ +4\upsilon_{pp}\upsilon_c E_c E_{pp} + (1+\upsilon_c)(1-2\upsilon_c)E_{pp}^2 \end{matrix}\right\}} \quad (7)$$

Here, E_c and ν_c are the elastic modulus and Poisson's ratio of the concrete matrix, while E_{PP} and ν_{PP} correspond to the properties of the PP inclusions. V_c and V_{PP} denote the volume fractions of concrete and PP, respectively. This model integrates the effect of Poisson's ratio, which influences the elastic response of PP-modified concrete composites. Unlike the traditional Voigt and Reuss models that neglect this parameter and may lead to less accurate predictions, the adopted Reuss–Voigt–Luo approach incorporates the Poisson effect by deriving improved relationships from the

fundamental elasticity equations. Consequently, the effective Poisson's ratios of the composite are determined as the following:

$$\begin{aligned} \upsilon_{hom}^{xy} &= \frac{\{V_c(1-\upsilon_{Gp})\upsilon_c + V_{Gp}(1-\upsilon_c)\upsilon_{Gp}\}\{V_c(1+\upsilon_{Gp})E_c + V_{Gp}(1+\upsilon_c)E_{Gp}\}}{\{V_c(1-\upsilon_{Gp}{}^2)E_c + V_{Gp}(1-\upsilon_c{}^2)E_{Gp}\}} \\ \upsilon_{hom}^{xz} &= \frac{\{V_c(1+\upsilon_{Gp}{}^2)E_c\upsilon_c + V_{Gp}(1+\upsilon_c{}^2)E_{Gp}\upsilon_{Gp}\}}{\{V_c(1-\upsilon_{Gp}{}^2)E_c + V_{Gp}(1-\upsilon_c{}^2)E_{Gp}\}} \\ \upsilon_{hom}^{zx} = \upsilon_{hom}^{zy} &= \frac{E_cE_{Gp}[V_c(1-\upsilon_{Gp})\upsilon_c + V_{Gp}(1-\upsilon_c)\upsilon_{Gp}]}{\left\{\begin{array}{c} E_cE_{Gp}[V_c^2(1-\upsilon_{Gp}) + V_{Gp}^2(1-\upsilon_c)] \\ +V_{Gp}V_c[(1+\upsilon_{Gp})(1-2\upsilon_{Gp})E_c^2 \\ +4\upsilon_{Gp}\upsilon_cE_cE_{Gp} + (1+\upsilon_c)(1-2\upsilon_c)E_{Gp}^2 \end{array}\right\}} \end{aligned} \quad (8)$$

The model ensures that the anisotropic interactions and the effect of Poisson's ratio are properly incorporated, providing an accurate estimate of the wall's mechanical behavior under multi-directional loading conditions. The corresponding effective Poisson's ratios (ν_{hom}) of the PP-reinforced concrete are computed as the volume-weighted contributions of the concrete matrix and the PP inclusions. However, it should be noted that this homogenization approach assumes a statistically homogeneous and macroscopically isotropic composite with randomly dispersed, non-agglomerated inclusions; therefore, local clustering effects and morphological irregularities are not explicitly captured in the present formulation. Based on these, the effective shear modulus (G_{hom}) and bulk modulus (K_{hom}) of the composite are derived using classical elasticity relations:

$$G_{hom}^{x} = E_{hom}^{x}[2(1+\nu_{hom})]^{-1}; G_{hom}^{y} = E_{hom}^{y}[2(1+\nu_{hom})]^{-1} \quad (9)$$

and;

$$K_{hom}^{x} = E_{hom}^{x}[3(1-2\nu_{hom})]^{-1}; K_{hom}^{y} = E_{hom}^{y}[3(1-2\nu_{hom})]^{-1} \quad (10)$$

2.2.2. Thermal Homogenization Using Maxwell–Eucken Model

The Maxwell–Eucken model is applied to estimate the effective thermal conductivity (λ_{hom}) of PP-reinforced concrete. The model is suitable for composites where one phase (PP) is dispersed as small, isotropic inclusions within a continuous matrix (concrete). This formulation is adopted because it is particularly appropriate for bi-phasic materials with low to moderate inclusion volume fractions and a clearly dominant continuous matrix, which corresponds to the present mixture configuration (PP ≤ 10%). Unlike more general self-consistent or symmetric approaches that treat both phases equivalently or are better suited for higher inclusion concentrations, the Maxwell–Eucken model explicitly represents a dispersed inclusion phase embedded within a continuous matrix. It therefore provides a physically consistent closed-form estimate of the effective conductivity for non-percolating composite systems. The effective thermal conductivity is expressed as [85]:

$$\lambda_{hom} = \lambda_c\{2\lambda_c + \lambda_{pp} - 2(\lambda_c - \lambda_{pp})v_{pp}\}\{2\lambda_c + \lambda_{pp} + 2(\lambda_c - \lambda_{pp})v_{pp}\}^{-1} \quad (11)$$

where λ_c and λ_{PP} denote the thermal conductivities of the concrete matrix and PP, respectively, and v_{PP} is the volumetric fraction of pumice powder, in which:

$$v_{PP} = 1 - v_c \quad (12)$$

The effective thermal expansion coefficient of the composite (α_{hom}) accounts for the contribution of both phases, reflecting the combined influence of the PP inclusions and the concrete matrix. It considers the relative volume fractions, the intrinsic thermal expansion properties of each phase (α_c for the concrete matrix and α_{pp} for the PP), and their interaction within the microstructure, providing a homogenized parameter that governs the wall's dimensional response under temperature variations.

$$\alpha_{hom} = (1 - v_{PP})\alpha_c + v_{PP}\alpha_{PP} \quad (13)$$

The thermal resistance (R_{hom}) of a wall of thickness (h_w) is defined as the ratio of the wall thickness to its effective thermal conductivity, providing a measure of the material's ability to resist heat flow. Mathematically, it is expressed as:

$$R_{hom} = \frac{h_w}{\lambda_{hom}} \tag{14}$$

where λ_{hom} is the effective thermal conductivity of the PP-modified concrete wall. This parameter quantifies how efficiently the wall impedes heat transfer, which is critical for evaluating its thermal performance and energy efficiency in structural applications.

Similarly, the thermal transmittance (U_{hom}) of the wall is defined as the inverse of its thermal resistance, representing the rate of heat transfer through the wall per unit area under a temperature difference. It is expressed as:

$$U_{hom} = \frac{1}{R_{hom}} = \frac{\lambda_{hom}}{h_w} \tag{15}$$

where λ_{hom} is the effective thermal conductivity of the PP-modified concrete and h_w is the wall thickness. This parameter provides a practical measure of the wall's ability to conduct heat, which is essential for assessing thermal efficiency and energy performance in building and structural applications.

Finally, the thermal flux (ϕ_{hom}) through the wall represents the amount of heat transferred per unit area due to a temperature difference between the wall surfaces. It is expressed as:

$$\phi_{hom} = U_{hom}(T_{int} - T_{ext}) \tag{16}$$

where U_{hom} is the thermal transmittance of the PP-modified concrete wall, T_{int} is the interior temperature, and T_{ext} is the exterior temperature. This parameter provides a direct measure of the wall's thermal performance and efficiency, capturing how effectively the material regulates heat flow under operational conditions.

The Maxwell–Eucken model assumes that the dispersed PP inclusions are small, isotropic, and uniformly distributed within a continuous concrete matrix. It also presumes linear heat conduction and neglects particle clustering or agglomeration effects. Consequently, the model provides an approximate estimate of the effective thermal conductivity and expansion, which may be less accurate for high PP fractions, non-uniform microstructures, or extreme temperature gradients.

2.3. Governing Equations for Thermo-Mechanical Response

The PP-modified concrete wall is represented as a homogeneous equivalent plate with effective thermo-elastic properties obtained from the Reuss–Voigt–Luo and Maxwell–Eucken homogenization schemes. The governing equations account for in-plane and transverse shear effects, ensuring consistent interaction between mechanical displacements and thermal strains.

$$\int_0^t (\delta\chi - \delta Y)dt = 0 \tag{17}$$

The mechanical bending response is derived using the principle of virtual work, which balances the virtual internal strain energy with the work of external forces. This formulation captures both bending and shear deformations, while incorporating thermal effects through the homogenized elastic and thermal properties. The virtual variation of the internal strain energy, denoted as $\delta\chi$, is expressed as follows and accounts for the contributions of both bending and shear deformations within the PP-modified concrete panel:

$$\delta\chi = \int_0^A \int_{-h/2}^{h/2} \left(\sigma_x \delta\varepsilon_x + \sigma_y \delta\varepsilon_y + \tau_{xy}\delta\gamma_{xy} + \tau_{yz}\delta\gamma_{yz} + \tau_{xz}\delta\gamma_{xz}\right) dAdz \tag{18}$$

By substituting Eq. (4) into Eq. (19), the resulting expression becomes:

$$\delta\chi = \int_A \begin{pmatrix} N_x \dfrac{\partial \delta u_0}{\partial x} - M_x^b \dfrac{\partial^2 \delta w_b}{\partial^2 x} + M_x^s \dfrac{\partial^2 \delta w_s}{\partial^2 x} \\ +N_y \dfrac{\partial \delta v_0}{\partial y} - M_y^b \dfrac{\partial^2 \delta w_b}{\partial^2 y} + M_y^s \dfrac{\partial^2 \delta w_s}{\partial^2 y} \\ +N_{xy}\left(\dfrac{\partial \delta u_0}{\partial y} + \dfrac{\partial \delta v_0}{\partial x}\right) + 2M_x^b \dfrac{\partial^2 \delta w_b}{\partial x \partial y} \\ +2M_x^s \dfrac{\partial^2 \delta w_s}{\partial x \partial y} + Q_{yz}\left(\dfrac{\partial \delta w_s}{\partial y}\right) + Q_{xz}\left(\dfrac{\partial \delta w_s}{\partial x}\right) \end{pmatrix} \tag{19}$$

The mechanical behavior of the PP-modified concrete panel is characterized by the following stress and moment resultants: the in-plane normal and shear forces (N), bending moments (M_b), shear-related moments (M_s), and transverse shear forces (Q). These quantities capture the panel's response to applied mechanical loads, including bending, shear, and in-plane stress distribution, providing a basis for evaluating deflections and mechanical stability.

$$N_{ij} = b\int_{-h_w/2}^{h_w/2} \sigma_{ij}\, dz; M_{ij}^b = b\int_{-h_w/2}^{h_w/2} z\sigma_{ij}\, dz; M_{ij}^s = b\int_{-h_w/2}^{h_w/2} f(z)\sigma_{ij}\, dz; Q_{ij} = b\int_{-h_w/2}^{h_w/2} g(z)\sigma_{ij}\, dz. \tag{20}$$

Note that the indices i and j correspond to the in-plane directions x or y. The term $\delta\Upsilon$ represents the virtual work of the external forces acting on the panel. It accounts for both mechanical buckling loads, denoted by N_b, and thermal loads, denoted by T. Specifically, δV quantifies the virtual external energy induced by these applied loads and serves as the counterpart to the internal virtual strain energy, enabling the formulation of equilibrium conditions within the principle of virtual work.

$$\delta\Upsilon = -\int_A \int_{\frac{-h}{2}}^{\frac{h}{2}} N_b(\delta w_b + \delta w_s)\, dAdz = -\int_A \int_{-h/2}^{h/2} T(\delta w_b + \delta w_s)\, dAdz \tag{21}$$

By substituting Eqs. (20) and (22) into Eq. (18), which itself incorporates the thermal and mechanical contributions expressed in Eq. (20), and performing integration by parts while taking into account the virtual variations δu_0, δv, δw_b, and δw_s, the resulting governing equations of motion for the PP-modified concrete panel are obtained. These equations describe the coupled bending, shear, and thermal responses of the panel under combined mechanical and thermal loading conditions, capturing the influence of both material heterogeneity and geometric effects.

$$\begin{aligned} &\delta u_0: \frac{\partial N_x}{\partial x} + \frac{\partial N_{xy}}{\partial y} = 0 \\ &\delta v_0: \frac{\partial N_y}{\partial y} + \frac{\partial N_{xy}}{\partial x} = 0 \\ &\delta w_b: \left(\frac{\partial^2 M_x^b}{\partial x^2} - 2\frac{\partial^2 M_{xy}^b}{\partial x \partial y} + \frac{\partial^2 M_y^b}{\partial y^2}\right) + N_b = 0 \\ &\delta w_s: \left(\frac{\partial^2 M_x^s}{\partial x^2} - 2\frac{\partial^2 M_x^s}{\partial x \partial y} + \frac{\partial^2 M_y^s}{\partial y^2}\right) + \left(\frac{\partial Q_{xz}}{\partial x} + \frac{\partial Q_{yz}}{\partial y}\right) + N_b = 0 \end{aligned} \tag{22}$$

The stress resultants, expressed in terms of material stiffness and displacement components, can be derived as shown in Appendix A. Thermal effects are represented by the corresponding thermal resultants induced by temperature gradients across the panel's thickness. These include in-plane thermal forces (N_T), thermal bending moments (M_{Tb}), thermal shear moments (M_{Ts}), and transverse shear forces due to thermal expansion (Q_T). These terms account for the coupling between thermal strains and mechanical displacements, enabling the assessment of thermal buckling, stress variation, and overall thermo-mechanical performance of the PP-modified concrete panel.

$$N_{Tij} = b\int_{-h_w/2}^{h_w/2} \tilde{Q}_{11}\, \alpha_{hom} T dz \tag{23}$$

$$M_{Tij}^{b} = b\int_{-h_w/2}^{h_w/2} z\tilde{Q}_{11}\,\alpha_{hom}Tdz$$
$$M_{Tij}^{s} = b\int_{-h_w/2}^{h_w/2} f(z)\tilde{Q}_{11}\,\alpha_{hom}Tdz$$

The buckling loads of the simply supported rectangular panel correspond to the critical in-plane forces at which the panel loses stability under compressive or thermal stresses. These loads are determined by solving the governing equations of motion derived from the principle of virtual work, incorporating both the mechanical stiffness and the thermal expansion effects of the PP-modified concrete.

$$N_b = N_{bx} + \eta N_{by} \tag{24}$$

In Eq. (25a), N_b represents the total critical buckling load of the panel under combined uni-axial or bi-axial loading. The terms N_{bx} and N_{by} correspond to the contributions of the axial loads applied along the x- and y-directions, respectively. The parameter η is the bi-axial load coefficient, defining the ratio of the axial load in the y-direction to that in the x-direction: $\eta = 0$ corresponds to uni-axial buckling along the x-direction, while $\eta = 1$ represents bi-axial buckling with equal loads in both directions. For a square rectangular wall, the in-plane normal forces along the x and y directions are equal, and the associated transverse shear forces are also equal. That is:

$$N_{bx} = T_x = N_{by} = T_x \tag{25}$$

2.4. Analytical Solution Using Navier's Method

For the simply supported rectangular panel with length a, width b, and total thickness h_w, the boundary conditions enforce zero transverse displacement and bending moments along all edges. Specifically, at $x = 0$ and $x = a$, as well as $y = 0$ and $y = b$, the deflection w and rotations vanish, while the in-plane displacements u_0 and v_0 are constrained according to the support type. These conditions allow edge rotation while preventing vertical displacement, consistent with classical simply supported behavior under mechanical and thermal loading:

$$\begin{aligned} &x = 0\ and\ x = a : v_0 = w_b = w_s = N_x = M_x^b = M_x^s = 0 \\ &y = 0\ and\ y = b : u_0 = w_b = w_s = N_y = M_y^b = M_y^s = 0 \end{aligned} \tag{26}$$

To enable a tractable analytical solution, the PP-modified concrete panel is assumed homogeneous and linearly elastic with small deformations, and its simply supported edges allow rotation while preventing transverse displacement, consistent with Eq. (26). Thermal and mechanical effects are considered linearly coupled and superimposed. For clarity and reproducibility, the key model assumptions are summarized as follows:

- Linear elasticity: Material response is proportional to applied loads.
- Small deformations: Geometric nonlinearity is neglected.
- Simply supported boundaries: Edges allow rotation but no transverse displacement.
- Thermal–mechanical superposition: Thermal and mechanical effects are linearly combined.

These assumptions enable the use of Navier-type solutions, where double Fourier series satisfy boundary conditions exactly, providing an accurate evaluation of the panel's mechanical and thermal response.

By considering Navier solutions, the in-plane displacements $u_0(x, y)$ and $v_0(x, y)$, together with the transverse bending $w_b(x, y)$ and shear $w_s(x, y)$ components, are represented as sums of sinusoidal functions along both axes. Each term corresponds to a specific half-wave in the x and y directions, transforming the governing partial differential equations into algebraic equations for the Fourier coefficients. This approach enables analytical determination of deflections, stress resultants, and critical buckling loads, while allowing efficient evaluation of multiple parameters, including PP content, panel dimensions, and thermal loads. The displacement components are expressed as double Fourier series:

$$u(x,y) = \sum_{n=1}^{\infty}\sum_{m=1}^{\infty} X_{mn} cos(\xi x)\, sin(\varsigma y) \tag{27.a}$$

$$v(x,y) = \sum_{n=1}^{\infty}\sum_{m=1}^{\infty} Y_{mn} sin(\xi x)\, cos(\varsigma y) \tag{27.b}$$

$$w_b(x,y) = \sum_{n=1}^{\infty}\sum_{m=1}^{\infty} Z_{bmn} sin(\xi x)\, sin(\varsigma y) \tag{27.c}$$

$$w_s(x,y) = \sum_{n=1}^{\infty}\sum_{m=1}^{\infty} Z_{smn} sin(\xi x)\, sin(\varsigma y) \tag{27.d}$$

Here, $X_{mn}, Y_{mn}, Z^b_{mn}, Z^s_{mn}$ represent the unknown Fourier coefficients corresponding to the in-plane displacements (u_0, v_0) and the bending and shear components of the transverse displacement (w_b, w_s), respectively. These coefficients are determined by substituting the series expansions into the governing equations of motion and solving the resulting algebraic system.

$$\xi = \frac{m\pi}{a};\ \varsigma = \frac{n\pi}{b} \tag{28}$$

Each coefficient captures the contribution of the (m,n)-th half-wave in the x and y directions, ensuring that both the boundary conditions and the coupled thermo-mechanical behavior of the PP-modified concrete panel are accurately satisfied.

by substituting the Navier series expansions for displacements into the governing equations and assembling the contributions from all modes, the coupled thermo-mechanical behavior of the PP-modified concrete panel can be expressed compactly in matrix form as:

$$\left(\begin{bmatrix} k_{11} & k_{12} & k_{13} & k_{14} \\ k_{21} & k_{22} & k_{23} & k_{24} \\ k_{31} & k_{32} & k_{33} & k_{34} \\ k_{41} & k_{42} & k_{43} & k_{44} \end{bmatrix} - N \begin{bmatrix} 0 & 0 & 0 & 0 \\ 0 & 0 & 0 & 0 \\ 0 & 0 & N_{33} & 0 \\ 0 & 0 & 0 & \eta \end{bmatrix}\right) \begin{Bmatrix} X_{mn} \\ Y_{mn} \\ Z_{bmn} \\ Z_{smn} \end{Bmatrix} = \begin{Bmatrix} 0 \\ 0 \\ 0 \\ 0 \end{Bmatrix} \tag{29}$$

where $[K]$ is the global stiffness matrix incorporating both mechanical and thermal effects, $[X]$ is the vector of unknown displacement coefficients $\left(X_{mn}, Y_{mn}, Z^b_{mn}, Z^s_{mn}\right)$. The main blocks of $[K]$ correspond to bending, shear, and in-plane stiffness contributions, while off-diagonal terms represent the coupling between thermal expansions and mechanical loads, enabling the panel's thermo-mechanical interaction to be captured. This formulation enables the analytical determination of deflections, bending moments, shear forces, and critical buckling loads of the simply supported PP-reinforced panel.

It is recommended to adopt a reduced system of equations by retaining only the dominant terms or lower-order modes in the Navier series. This simplification preserves the essential characteristics of the panel's thermo-mechanical response while significantly reducing computational complexity and facilitating analytical solution.

$$\left(\begin{bmatrix} k_{33} - N_{33} & k_{34} \\ k_{43} & k_{44} \end{bmatrix}\right) \begin{Bmatrix} w_{bmn} \\ w_{smn} \end{Bmatrix} = \begin{Bmatrix} 0 \\ 0 \end{Bmatrix} \tag{30}$$

To solve the problem and determine the critical buckling loads of the system, the determinant of the reduced stiffness matrix is computed. This procedure yields the eigenvalues corresponding to the buckling loads for the simply supported PP-modified concrete wall.

$$N = solve\left(det \begin{bmatrix} k_{33} - N_{33} & k_{34} \\ k_{43} & k_{44} \end{bmatrix}\right) \tag{31}$$

The explicit expressions of the stiffness matrix elements K_{ij}, derived considering the simply supported boundary conditions, are given by:

$$
\begin{aligned}
&K_{11} = -A_{11}\xi^2 - A_{66}\varsigma^2; K_{12} = -A_{12}\xi\varsigma - A_{66}\eta\varsigma;\ K_{13} = B_{11}\xi^3 + B_{12}\xi\varsigma^2 + 2B_{66}\xi\varsigma^2;\\
&K_{14} = B^s_{11}\xi^3 + B^s_{12}\xi\varsigma^2 + 2B^s_{66}\xi\varsigma^2;\\
&K_{23} = B_{22}\varsigma^3 + B_{12}\varsigma\xi^2 + 2B_{66}\varsigma\xi^2;\ S_{24} = B^s_{11}\varsigma^3 + B^s_{12}\varsigma\xi^2 + 2B^s_{66}\varsigma\xi^2;\\
&K_{33} = -D_{11}\xi^4 - 2\xi^2\varsigma^2(2D_{66} + D_{12}) - D_{22}\varsigma^2;\\
&S_{44} = -H^s_{11}\xi^4 - 2\xi^2\varsigma^2(2H^s_{66} + H^s_{12}) - H^s_{22}\varsigma^2 - A^s_{44}\xi^2 - A^s_{55}\varsigma^2.
\end{aligned}
\tag{32}
$$

The developed analytical framework provides a direct link between material-level modifications and structural performance, enabling engineers to predict both mechanical stability and thermal behavior of PP-modified concrete walls. By quantifying critical mechanical and thermal buckling thresholds, as well as effective thermal resistance, transmittance, and heat flux, this model supports the design of lightweight concrete walls that meet energy efficiency and structural safety requirements. Such predictive capability is particularly relevant for sustainable building applications, where balancing stiffness, stability, and thermal insulation is essential for optimizing performance under combined mechanical and environmental loading conditions.

3. Results and Discussion

This section presents an analytical evaluation of the thermomechanical performance of PP-modified concrete walls. The study examines how the addition of pumice powder influences the elastic, thermal, and coupled responses of the composite wall under simple support conditions. The results are discussed in terms of material properties, stress distribution, deformation behavior, and thermal effects, yielding information on the effectiveness of PP as a partial substitute in concrete mixtures.

3.1. Thermo-Elastic Properties of Constituent Materials

The thermo-elastic properties of the concrete matrix and PP used in this study are summarized in Table 3. These properties form the basis for the homogenization and subsequent evaluation of the wall's coupled mechanical and thermal response.

Table 3. Thermo-elastic properties of the concrete matrix and pumice powder (PP) used in the analysis

Material	Ref	Elastic Modulus E[GPa]	Poisson's Ratio ν	Thermal Conductivity λ[W·m^{-1}·°C^{-1}]	Thermal Expansion α[×10^{-6}/°C]
Concrete Matrix	Neville and Brooks [86]	20	0.3	1.75	13.5
Pumice Powder	Bilir et al. [87]	7–10	0.25–0.29	0.25–0.45	4–6

Based on the thermo-elastic properties summarized in Table 3, the inclusion of PP is expected to influence the wall's behavior due to its lower stiffness, reduced thermal conductivity, and moderated thermal expansion compared to the concrete matrix. Its vesicular microstructure and pozzolanic composition suggest that PP may act as compliant, low-conductivity inclusions, potentially redistributing stresses and altering heat transfer paths within the concrete. Consequently, the wall may exhibit slightly reduced stiffness, improve thermal insulation, and mitigate differential expansion under temperature gradients, effects that will be systematically evaluated in the subsequent homogenization and high-order deformation analysis.

3.2. Validation of the Homogenization Model

To verify the accuracy of the proposed homogenization approach, a comparative validation is carried out using the experimental data reported by Kalkan and Gündüz [88]. In their work, ordinary concrete was partially replaced with pumice aggregates at different volume fractions, and the corresponding variations in Young's modulus were experimentally measured, as illustrated in Fig. 5.

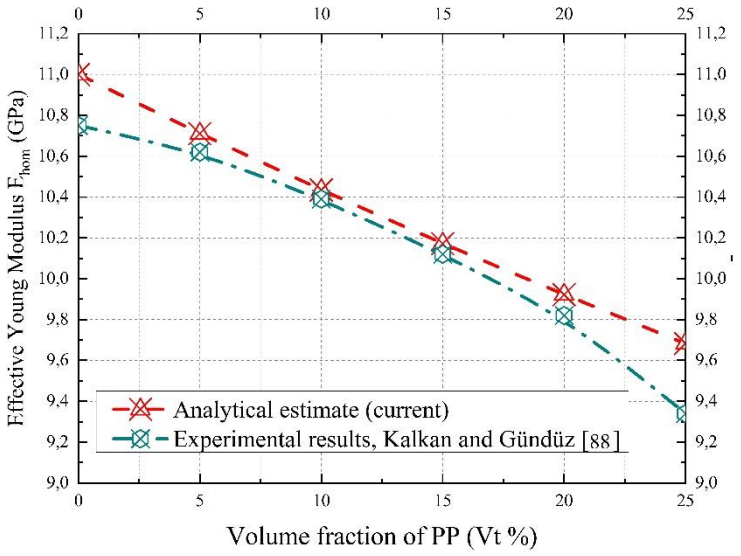

Fig. 5. Comparison between the predicted elastic modulus from the proposed homogenization model and experimental results reported by Kalkan and Gündüz [88] for concrete reinforced with different pumice powder fractions.

For this validation, the material properties are chosen to be consistent with those adopted in the reference study. Specifically, the ordinary concrete is characterized by an elastic modulus of 11 GPa and a Poisson's ratio of 0.2, while the pumice particles exhibit an elastic modulus of 5 GPa and a Poisson's ratio of 0.15.

A close agreement can be observed between the analytical predictions and the experimental data, particularly when the volume fraction of pumice powder (PP) ranges between 5% and 20% of the total mix, confirming the reliability of the proposed model within this composition range. For a PP content of 12%, the discrepancy between analytical and experimental results is below 1%, indicating excellent agreement. For lower (0%) or higher (25%) PP content, the error reaches a maximum of approximately 4%, which remains within acceptable limits for engineering applications. These quantitative indicators demonstrate the predictive capability of the analytical model for mechanical behavior.

The reduction in elastic modulus predicted for pumice contents lies within the stiffness reduction factors (0.6–0.7 of the gross stiffness) already adopted in Eurocode 2 and ACI 318 for cracked and lightweight concretes, indicating that the associated reduction in buckling resistance remains within standard design safety margins [89].

The validation of the analytical model for thermal expansion is carried out using the experimental data reported by Şevket Onur Kalkan and Lütfullah Gündüz [88], as illustrated in Fig. 6(a). The coefficient of thermal expansion of pumice is taken as 10×10^{-6} /°C, while that of lightweight concrete is approximately 1×10^{-6} /°C. For conventional concrete, a reference value of 7×10^{-6} /°C is adopted. The analytical results show excellent agreement with the experimental data, particularly for pumice powder (PP) volume fractions between 5% and 10%, where the discrepancy between analytical predictions and experimental measurements is approximately 1%. Beyond this range, the accuracy of the homogenization model slightly decreases but remains acceptable, with errors reaching around 3%, likely due to the increasing influence of the highly porous pumice phase on the composite's thermal response.

Similarly, the validation of thermal conductivity is performed based on the same reference study [29], with results presented in Fig. 6(b). The thermal conductivity of pumice reinforcement is taken as 0.1 W/(m·°C), while that of the concrete matrix is 1.8 W/(m·°C). The analytical model predictions are compared with an experimental reference value of 0.62 W/(m·°C) for lightweight concrete. The results show that a small error of around 5% starts to appear when the PP volume fraction reaches 3% and above, but overall, the model reliably captures the thermal transport behavior of PP-modified concrete.

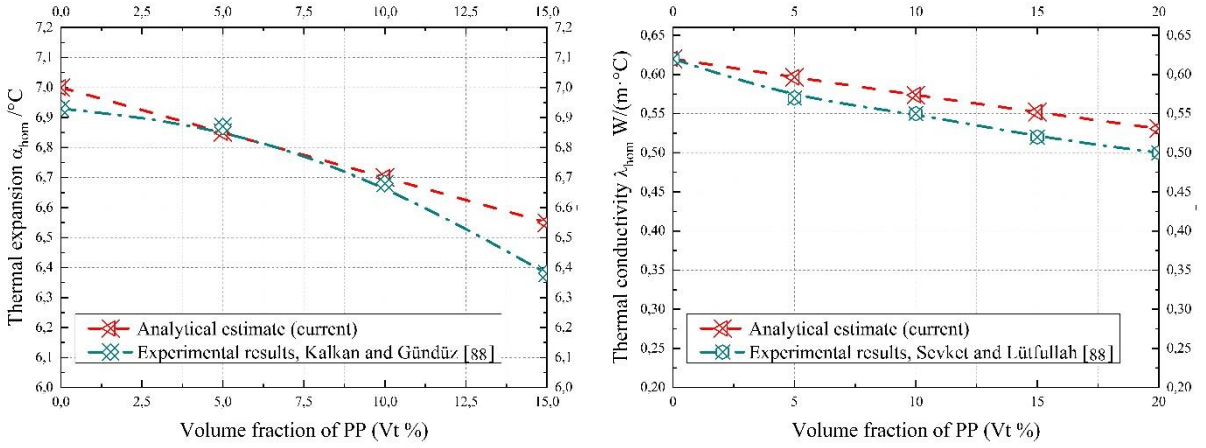

(a) Expansion coefficient (b) Thermal conductivity

Fig. 6. Comparison between analytical predictions and experimental data of the effective thermal properties of PP modified concrete [88], including the effective thermal expansion coefficient (α_{hom}) and the effective thermal conductivity (λ_{hom})

The adoption of identical constituent properties to those reported experimentally is necessary to ensure comparability of the physical system and should not be interpreted as parameter fitting. The homogenization model contains no adjustable empirical coefficients, and no inverse identification procedure was performed. Consequently, the agreement observed reflects the intrinsic predictive capability of the theoretical formulation rather than calibration against experimental data.

3.3. Mechanical Behavior of PP-Modified Concrete Walls

To analyze the mechanical behavior of the PP-modified concrete walls, the critical buckling load is expressed in a non-dimensional form. This approach allows the results to be generalized and compared across different wall geometries and PP contents. The non-dimensional critical buckling load N_{cr} is defined as:

$$N_{cr} = \frac{12(1-\nu_c)a^2N}{E_c h_w^3} \tag{35}$$

Table 4. Dimensionless mechanical buckling loads of simply supported PP-modified concrete walls for varying volume fractions of pumice powder (0–10%) and different length-to-thickness ratios (a/hw), under uni-axial (η = 0) and bi-axial (η = 1) loading conditions, (a=b)

		Uni-axial buckling load η = 0					Bi-axial buckling loads η = 1				
		Volume fraction of PP inclusions (v_{PP})									
		0%	2.5%	5%	7.50%	10%	0%	2.5%	5%	7.50%	10%
length-to-thickness ratios (a/h_w) of the plate	5	2.9253	2.7530	2.6013	2.4657	2.3448	1.4626	1.3765	1.3006	1.2328	1.1724
	10	3.4136	3.2175	3.0453	2.8917	2.7550	1.7068	1.6088	1.5226	1.4458	1.3775
	15	3.5227	3.3215	3.1449	2.9874	2.8474	1.7614	1.6608	1.5724	1.4937	1.4237
	20	3.5626	3.3595	3.1813	3.0225	2.8813	1.7813	1.6798	1.5907	1.5112	1.4406
	25	3.5814	3.3774	3.1985	3.0390	2.8972	1.7907	1.6887	1.5992	1.5195	1.4486
	30	3.5917	3.3872	3.2079	3.0480	2.9060	1.7958	1.6936	1.6039	1.5240	1.4530
	35	3.5979	3.3932	3.2136	3.0535	2.9113	1.7989	1.6966	1.6068	1.5267	1.4556
	40	3.6019	3.3971	3.2173	3.0570	2.9147	1.8010	1.6985	1.6086	1.5285	1.4573
	45	3.6047	3.3997	3.2198	3.0595	2.9171	1.8024	1.6999	1.6099	1.5297	1.4585
	50	3.6067	3.4016	3.2216	3.0613	2.9188	1.8034	1.7008	1.6108	1.5306	1.4594

Table 4 presents the dimensionless mechanical buckling coefficients of simply supported square concrete walls reinforced with pumice powder (PP) under uni-axial (η = 0) and bi-axial (η = 1) loading, with aspect ratios (a/h_w) ranging from 5 to 50 and PP volume fractions from 0% to 10%.

The data show a systematic decrease in buckling loads with increasing PP content. For example, at a/h_w = 10 under uni-axial loading, the critical buckling coefficient decreases from 3.414 for plain concrete to 2.755 at 10% PP, a reduction of approximately 19%, reflecting the direct impact of reduced modulus of elasticity due to PP incorporation. Similarly, under bi-axial loading, the coefficient decreases from 1.707 to 1.378, showing a 19% reduction, confirming that biaxial compression is more sensitive to stiffness reduction.

The percentage reduction in buckling load due to PP incorporation remains nearly constant (≈19–20%) across all aspect ratios, indicating that the influence of PP content on mechanical stability is largely independent of plate slenderness. This suggests that stiffness degradation caused by PP inclusions proportionally affects the critical load without altering the geometric sensitivity of the plate. Uni-axial buckling loads are consistently higher than bi-axial ones for all PP fractions and aspect ratios. This confirms classical plate theory predictions: bi-axial compression promotes earlier instability, and the relative difference increases slightly with PP content due to the larger influence of compliance on combined in-plane stresses. Even low PP fractions (2.5–5%) produce measurable reductions (~5–10%) in critical loads, suggesting that even moderate cement replacement affects wall stability. This underscores the importance of accounting for PP content in design to balance thermal efficiency gains with mechanical stability.

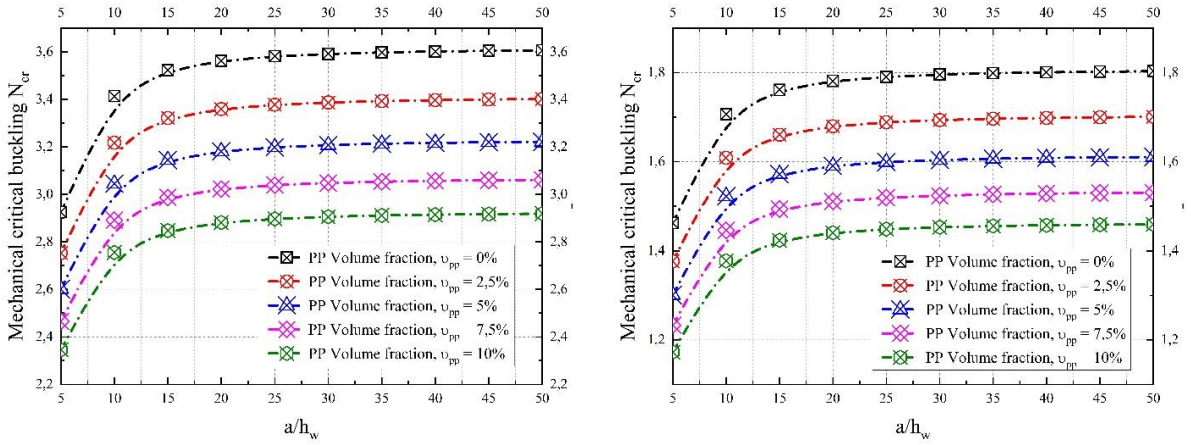

(a) Uni-axial buckling load, η = 0

(b) Bi-axial buckling loads, η = 1

Fig. 7. Variation of the critical buckling load of a square PP modified concrete wall ($a = b$), with the length to thickness ratio (a/h_w) and pumice powder volume fraction under uni-axial buckling conditions (η = 0), and bi-axial buckling conditions (η = 1)

Fig. 7 illustrates the effect of pumice powder (PP) content on the buckling behavior of a square concrete wall. It is evident that increasing the PP volume fraction reduces the wall's stiffness, resulting in lower critical buckling loads for both uni-axial (η = 0) and bi-axial (η = 1) loading conditions. The trend highlights that higher PP content, due to its lower elastic modulus compared to the concrete matrix, diminishes the wall's mechanical stability, making it more susceptible to buckling under compressive loads. This effect is more pronounced at higher length-to-thickness ratios, where the wall becomes increasingly flexible.

Fig. 8 presents the variation of the critical buckling load of a rectangular plate $\left(a = \sqrt{b}\right)$with respect to the length-to-thickness ratio and the volumetric fraction of pumice powder (PP). Similar to the square plate case, an increase in PP content leads to a noticeable reduction in the critical buckling load under both uni-axial (η = 0) and bi-axial (η = 1) conditions. This reduction indicates that incorporating more PP weakens the stiffness of the composite plate, making it less resistant to instability. Moreover, the influence of PP becomes more significant as the slenderness ratio increases. These results highlight a trade-off between reduced weight and mechanical stability. Increasing PP content lowers stiffness and critical buckling loads, especially for slender panels, indicating that wall geometry and PP fraction must be carefully balanced. Practically, maintaining PP contents within 5–10% ensures sufficient buckling resistance while benefiting from lightweight and thermally efficient concrete, guiding sustainable and safe wall design.

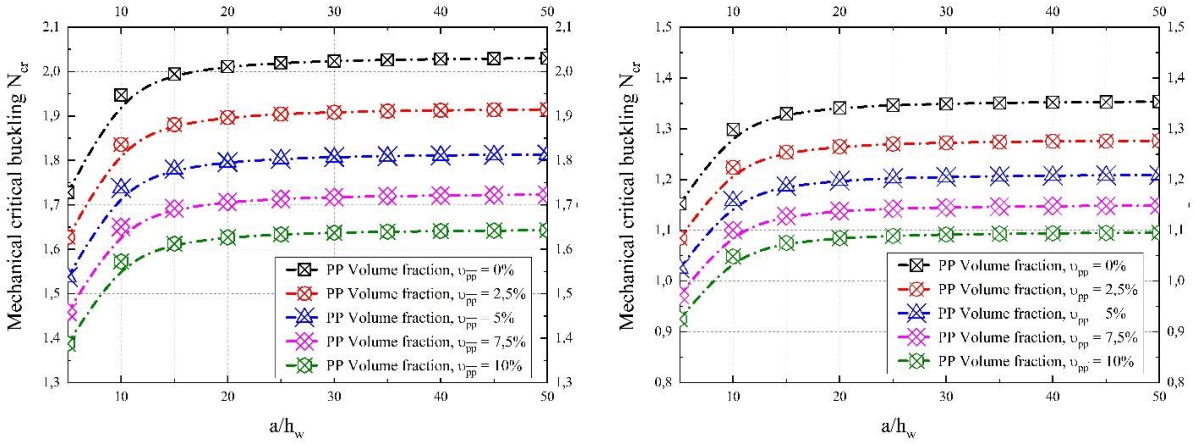

(a) Uni-axial buckling load, η = 0 (b) Bi-axial buckling loads, η = 1

Fig. 8. Critical buckling load of a rectangular plate $(a = \sqrt{b})$ as a function of the length-to-thickness ratio and the volumetric fraction of PP, considering uni axial buckling with η = 0 and bi axial buckling with η = 1

To quantify the robustness of the predicted buckling response, a local sensitivity analysis was performed using the normalized coefficient $S_X^Y = (\Delta Y/Y_0)/(\Delta X/X_0)$, where $Y = \bar{N}_{cr}$ and X denotes a material parameter. Using a baseline mixture with $V_{PP} = 5\%$, the governing stiffness relation $D \propto Eh^3$ implies $S_E^{\bar{N}cr} \approx 1$, confirming that the buckling capacity varies almost linearly with the effective elastic modulus. In contrast, since thermal conductivity does not enter the mechanical stiffness matrix, $S_k^{\bar{N}cr} \approx 0$. The pumice volume fraction exhibits a moderate sensitivity $S_{V_{PP}}^{\bar{N}cr}$, as it reduces E through homogenization, leading to the gradual decrease observed in Fig. 5.

3.4. Thermal and Coupled Thermo-Mechanical Behavior of PP-Modified Concrete Walls

In this section, the influence of pumice powder incorporation on the thermal performance of concrete walls is investigated. The analysis focuses on the coupled thermo-mechanical response of the slab, where temperature gradients induce additional stresses and potential deformations, the study aims to evaluate the effectiveness of pumice powder in enhancing the thermal insulation capacity and reducing thermally induced instability in concrete elements.

3.4.1. Thermal Resistance (R) of a Concrete Panel Reinforced with PP

The thermal resistance (R) represents the ability of a material or structural element to resist heat flow across its thickness. It is a key indicator of thermal insulation performance and is defined as the ratio between the wall thickness and its effective thermal conductivity. In the present study, the thermal resistance of the pumice powder (PP)–modified concrete panel is evaluated to quantify the improvement in insulation capacity resulting from the inclusion of PP.

Given the inherently low thermal conductivity of pumice powder (approximately 0.25–0.45 W/(m·°C)) compared to conventional concrete (about 1.75 W/(m·°C)), an increase in PP content is expected to enhance the overall thermal resistance of the wall. The analytical results presented here aim to establish the relationship between the volumetric fraction of PP and the corresponding rise in thermal resistance, emphasizing the potential of pumice-modified concrete for thermally efficient building envelopes.

Table 5 presents the variation of thermal resistance R for concrete panels reinforced with different volumetric fractions of pumice powder (PP), considering wall thicknesses ranging from 5 cm to 50 cm. The results reveal a clear trend: for any given wall thickness, the thermal resistance increases progressively with higher PP content. This improvement is attributed to the inherently low thermal conductivity of pumice, which reduces the effective heat transfer across the composite. On average, incorporating 10% PP enhances the thermal resistance by approximately 18–21% compared to

plain concrete, confirming the positive influence of PP addition on the thermal performance of the material.

Table 5. Variation of thermal resistance (R) of pumice powder (PP)-modified concrete panels with wall thickness (h_w) and volumetric fraction of PP

Volume fraction of PP inclusions (v_{PP})	Thermal Resistance (R) W/(m·°C)				
	(h_w=5cm)	(h_w=10cm)	(h_w=15cm)	(h_w=20cm)	(h_w=25cm)
0%	0.028	0.056	0.083	0.111	0.139
2.5%	0.029	0.058	0.087	0.116	0.145
5%	0.030	0.061	0.091	0.122	0.152
7.5%	0.032	0.064	0.096	0.128	0.159
10%	0.033	0.067	0.100	0.134	0.167
Volume fraction of PP inclusions (v_{PP})	(h_w=30cm)	(h_w=35cm)	(h_w=40cm)	(h_w=45cm)	(h_w=50cm)
0%	0.167	0.194	0.222	0.250	0.278
2.5%	0.175	0.204	0.233	0.262	0.291
5%	0.183	0.213	0.244	0.274	0.305
7.5%	0.191	0.223	0.255	0.287	0.319
10%	0.200	0.234	0.267	0.301	0.334

Moreover, R increases almost linearly with wall thickness, as expected from the direct proportionality $R = h_w/\lambda_{\text{hom}}$. For instance, when the thickness increases from 5 cm to 50 cm, the thermal resistance of unmodified concrete rises from 0.028 to 0.278 (around 18%), representing nearly a tenfold increase. This linear relationship demonstrates that both material composition and geometric configuration significantly affect the heat-insulating capacity of the wall.

The combined effect of PP reinforcement and increased wall thickness leads to a noticeable enhancement in thermal insulation. The inclusion of up to 10% PP yields a meaningful gain in resistance across all thicknesses, making pumice-modified concrete a promising material for thermally efficient building envelopes, particularly in energy-sensitive structural applications.

These results highlight the practical benefits of PP-modified concrete for building design. The progressive increase in thermal resistance with PP content demonstrates that pumice incorporation effectively improves insulation, reducing heat transfer through walls. Combined with thicker wall sections, the material can enhance energy efficiency in buildings. This insight allows designers to optimize PP content and wall thickness to achieve a balance between structural performance, thermal efficiency, and sustainability.

3.4.2. Thermal Transmittance (U) of a Concrete Panel Reinforced with PP

Table 6 presents the calculated values of the thermal transmittance coefficient (U) for concrete panels incorporating different volumetric fractions of pumice powder (PP), considering wall thicknesses ranging from 5 cm to 50 cm. The results show that the U-value decreases with both increasing PP content and wall thickness, indicating an improvement in the insulation capacity of the concrete panels.

For a fixed wall thickness, the inclusion of PP reduces the overall heat transfer through the panel due to the low thermal conductivity of pumice compared to that of conventional concrete. For instance, at a thickness of 10 cm, the U-value decreases from 18.00 W/m^2·°C for unmodified concrete to approximately 14.97 W/m^2·°C when 10% PP is added—representing a reduction of around 17%. This trend confirms the beneficial role of pumice in lowering the material's thermal transmittance. Additionally, the results highlight the strong dependence of U on wall thickness. As the panel becomes thicker, thermal transmittance drops significantly. For example, at 0% PP, increasing the wall thickness from 5 cm to 50 cm decreases the U-value from 36.00 to 3.60 W/m^2·°C, following an inverse proportionality consistent with $U = 1/R$. The combined effect of PP inclusion and increased wall thickness leads to a substantial enhancement in thermal insulation performance. These results suggest that pumice-modified concrete can effectively reduce heat

losses through structural walls, making it a sustainable material solution for energy-efficient building design.

Table 6. Variation of the thermal transmittance coefficient (U) of pumice powder (PP)-modified concrete panels with wall thickness (hw) and volumetric fraction of PP

Volume fraction of PP inclusions (v_{PP})	Thermal Transmittance (U) W/m^2·°C				
	(h_w=5cm)	(h_w=10cm)	(h_w=15cm)	(h_w=20cm)	(h_w=25cm)
0%	36.00	18.00	12.00	9.00	7.20
2.5%	34.38	17.19	11.46	8.60	6.88
5%	32.84	16.42	10.95	8.21	6.57
7.5%	31.36	15.68	10.45	7.84	6.27
10%	29.94	14.97	9.98	7.49	5.99
Volume fraction of PP inclusions (v_{PP})	(h_w=30cm)	(h_w=35cm)	(h_w=40cm)	(h_w=45cm)	(h_w=50cm)
0%	6.00	5.14	4.50	4.00	3.60
2.5%	5.73	4.91	4.30	3.82	3.44
5%	5.47	4.69	4.10	3.65	3.28
7.5%	5.23	4.48	3.92	3.48	3.14
10%	4.99	4.28	3.74	3.33	2.99

The results in Table 6 show a consistent reduction in thermal transmittance (U) with both increasing PP content and wall thickness. For instance, at a wall thickness of 20 cm, increasing PP content from 0% to 10% reduces the U-value from 9.00 to 7.49 W/m^2·°C, corresponding to a reduction of approximately 17%. A similar proportional decrease is observed across all thicknesses. Increasing wall thickness has a more pronounced effect: for plain concrete (0% PP), increasing thickness from 5 cm to 50 cm reduces the U-value from 36.00 to 3.60 W/m^2·°C (a 90% reduction), reflecting the inverse proportionality between U and thickness.

Although the incorporation of PP improves thermal performance, the resulting U-values (2.99–36.00 W/m^2·°C depending on thickness) remain higher than typical building envelope insulation requirements in many standards, which often require U-values below approximately 0.5–1.5 W/m^2·°C for exterior walls. Therefore, PP-modified concrete alone may not satisfy strict insulation criteria but can contribute to improved thermal resistance when combined with additional insulation layers. These results indicate that PP incorporation enhances thermal performance in a proportional and predictable manner, providing a basis for rational thickness selection when structural and thermal considerations must be balanced.

3.4.3. Thermal Flux (ϕ) of a Concrete Panel Reinforced with PP

Table 7 shows the computed thermal flux through a square concrete panel as a function of wall thickness and PP content. The results indicate that increasing the volumetric fraction of pumice powder consistently reduces the heat flux through the panel, demonstrating the insulating effect of PP. For a fixed panel thickness, the thermal flux decreases progressively with higher PP content. For example, at a thickness of 10 cm, the flux decreases from 504 W for unmodified concrete to approximately 419 W for a 10% PP inclusion, reflecting improved thermal resistance due to the low conductivity of pumice. Similarly, increasing the panel thickness significantly reduces the thermal flux for all PP fractions, following the expected inverse relationship between heat transfer and wall thickness. For instance, for 0% PP, the flux drops from 1008 W at 5 cm to 100.8 W at 50 cm, indicating that thicker panels are more effective in limiting heat transfer.

Table 8 presents the computed thermal flux through a square concrete panel under heating conditions, highlighting the effect of PP content and panel thickness on heat retention. The negative values indicate heat flow from the warmer interior to the colder exterior. As the PP volume fraction increases, the magnitude of heat flux decreases, reflecting the insulating effect of pumice. For example, at a panel thickness of 10 cm, the flux decreases from −756 W for unmodified concrete to approximately −629 W for a 10% PP inclusion, showing enhanced thermal resistance. Similarly, increasing panel thickness significantly reduces heat loss for all PP fractions. For instance, with 0%

PP, the flux drops from −1512 W at 5 cm to −151.2 W at 50 cm, indicating that thicker walls effectively reduce energy loss. The results demonstrate that incorporating pumice powder into concrete walls improves thermal insulation in cold climates, helping maintain indoor temperatures while reducing heating energy demand.

Table 7. Thermal flux (ϕ) through a 1×1 m^2 concrete panel reinforced with pumice powder (PP) in August, with external temperature 45°C and air-conditioned interior at 17°C, for varying panel thicknesses and PP volume fractions

Volume fraction of PP inclusions (v_{PP})	Thermal flux (ϕ) W				
	(h_w=5cm)	(h_w=10cm)	(h_w=15cm)	(h_w=20cm)	(h_w=25cm)
0%	1008.00	504.00	336.00	252.00	201.60
2.5%	962.73	481.36	320.91	240.68	192.55
5%	919.44	459.72	306.48	229.86	183.89
7.5%	878.02	439.01	292.67	219.50	175.60
10%	838.34	419.17	279.45	209.58	167.67
Volume fraction of PP inclusions (v_{PP})	(h_w=30cm)	(h_w=35cm)	(h_w=40cm)	(h_w=45cm)	(h_w=50cm)
0%	168.00	144.00	126.00	112.00	100.80
2.5%	160.45	137.53	120.34	106.97	96.27
5%	153.24	131.35	114.93	102.16	91.94
7.5%	146.34	125.43	109.75	97.56	87.80
10%	139.72	119.76	104.79	93.15	83.83

Table 8. Thermal flux (ϕ) through a 1×1 m^2 concrete panel reinforced with pumice powder (PP) in winter, with external temperature −6°C and heated interior at 36°C, for varying panel thicknesses and PP volume fractions

Volume fraction of PP inclusions (v_{PP})	Thermal flux (ϕ) W				
	(h_w=5cm)	(h_w=10cm)	(h_w=15cm)	(h_w=20cm)	(h_w=25cm)
0%	-1512.00	-756.00	-504.00	-378.00	-302.40
2.5%	-1444.09	-722.04	-481.36	-361.02	-288.82
5%	-1379.16	-689.58	-459.72	-344.79	-275.83
7.5%	-1317.03	-658.51	-439.01	-329.26	-263.41
10%	-1257.50	-628.75	-419.17	-314.38	-251.50
Volume fraction of PP inclusions (v_{PP})	(h_w=30cm)	(h_w=35cm)	(h_w=40cm)	(h_w=45cm)	(h_w=50cm)
0%	-252.00	-216.00	-189.00	-168.00	-151.20
2.5%	-240.68	-206.30	-180.51	-160.45	-144.41
5%	-229.86	-197.02	-172.40	-153.24	-137.92
7.5%	-219.50	-188.15	-164.63	-146.34	-131.70
10%	-209.58	-179.64	-157.19	-139.72	-125.75

These results confirm that the reduction in thermal flux with increasing PP content is directly associated with the decrease in effective thermal conductivity of the composite material. The incorporation of PP, characterized by its lower intrinsic conductivity and porous microstructure, disrupts continuous heat conduction pathways within the concrete matrix, increasing thermal resistance and limiting energy transfer. Since thermal flux is proportional to the effective conductivity and inversely proportional to wall thickness, the observed reductions reflect both material modification and geometric effects. Increasing panel thickness further elongates the heat transfer path, thereby reducing the temperature gradient per unit length and lowering the transmitted heat. The combined influence of altered conductivity pathways and increased conduction length explains the consistent reduction in heat flux under both cooling and heating conditions.

A sensitivity analysis of the steady-state heat transfer from tables 5 to 8, shows that the thermal resistance $R = h/k$ yields $S_k^R = -1$ and $S_k^\phi = 1$, meaning that a 10% reduction in thermal conductivity produces an approximately 10% increase in thermal resistance and a 10% decrease in heat flux. Since the effective conductivity is governed by the Maxwell–Eucken relation, the pumice volume fraction also exhibits a high sensitivity $S_{V_{PP}}^R$, confirming that pumice is the dominant driver of the observed thermal improvement.

3.4.4. Thermo-Mechanical Buckling of a Concrete Panel Reinforced with PP

To assess the combined effect of mechanical and thermal loads on PP-modified concrete panels, the critical thermo-mechanical buckling is evaluated using a quantitative approach that links the temperature gradient across the panel's thickness to the induced thermal stresses. The critical temperature distribution is expressed as:

$$T = \frac{\Delta T}{h_w}\left(\frac{h_w}{2} + z\right) + T_{ext};\ \Delta T = T_{int} - T_{ext} \tag{36}$$

The corresponding thermal in-plane force resultant N_T is computed by integrating the thermo-elastic response of the homogenized composite through the thickness:

$$N_T = \int_{-h_w/2}^{h_w/2} E_{hom}\alpha_{hom}\left(\frac{z}{h_w} + \frac{1}{2}\right) \tag{37}$$

Table 9. Critical thermal buckling temperature (ΔT_{cr}, °C) of a square concrete panel as a function of the length-to-thickness ratio (a/h_w) for varying volumetric fractions of pumice powder (PP), under uniaxial thermal loading (η = 0)

Critical thermal buckling ΔT_{cr} ($\times 10^2$)		Volume fraction of PP inclusions (v_{PP})				
		0%	2.5%	5%	7.50%	10%
length-to-thickness ratios (a/h_w) of the plate	5	39,7759	41,2369	42,7756	44,4079	46,1425
	10	11,3409	11,7733	12,2304	12,7165	13,2345
	15	5,1753	5,3742	5,5845	5,8085	6,0472
	20	2,9386	3,0519	3,1717	3,2993	3,4353
	25	1,8890	1,9619	2,0390	2,1212	2,2088
	30	1,3149	1,3657	1,4195	1,4767	1,5377
	35	0,9675	1,0049	1,0444	1,0865	1,1315
	40	0,7414	0,7701	0,8004	0,8327	0,8671
	45	0,5862	0,6088	0,6328	0,6584	0,6856
	50	0,4750	0,4934	0,5128	0,5335	0,5556

Table 9 presents the critical thermal buckling temperatures of square concrete panels reinforced with different volume fractions of pumice powder (0% to 10%) across a range of length-to-thickness ratios (a/h_w). It is observed that increasing the PP content leads to higher critical buckling temperatures for all panel thicknesses. For example, at a/h_w = 10, ΔT_{cr} increases from 1134 for unmodified concrete to 1323 for 10% PP, indicating that pumice inclusion enhances the panel's resistance to thermal buckling. Additionally, ΔT_{cr} decreases as the panel becomes thinner (higher a/h_w ratio), reflecting the higher susceptibility of slender panels to thermal instability. For instance, the critical temperature drops from ~3978 at a/h_w = 5 to ~47.5 °C at a/h_w = 50 for unmodified concrete.

Results in Table 9 demonstrate that incorporating pumice powder not only improves the mechanical properties but also enhances thermal stability, allowing concrete panels to better resist buckling under thermal loads, especially in moderately slender configurations. Fig. 9 illustrates that the critical thermal buckling temperature decreases with increasing panel slenderness (higher a/h_w), indicating that thinner panels are more susceptible to thermal instability. Moreover, an increase in the volumetric fraction of pumice powder generally reduces the panel's thermal resistance to buckling, as the lower stiffness of PP compared to the concrete matrix diminishes the structural rigidity under thermal loads.

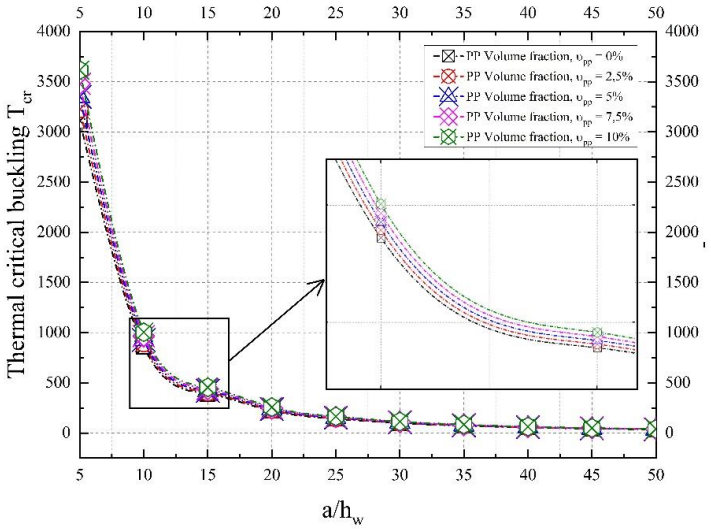

Fig. 9. Critical thermal buckling temperature of a rectangular PP-modified concrete panel ($a/b = \sqrt{2}$) as a function of the length-to-thickness ratio (a/h_w) and varying PP volume fractions

Fig. 10 shows that panels with a larger aspect ratio ($a/b = \sqrt{2}$) exhibit lower critical thermal buckling temperatures compared to square panels ($a/b = 1$), indicating that increasing panel elongation reduces stability under thermal loads. For both aspect ratios, the critical temperature decreases with increasing panel slenderness (a/h_w), highlighting the influence of thickness on thermal buckling resistance. These results emphasize the importance of geometric configuration in the thermo-mechanical performance of PP-modified concrete panels.

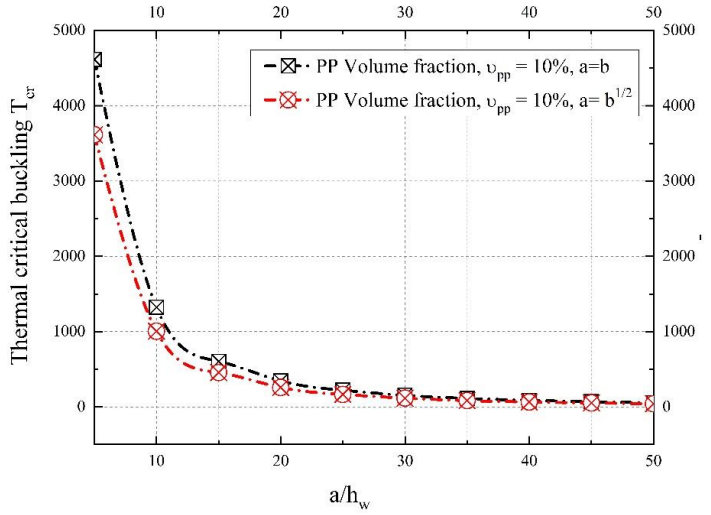

Fig. 10. thermal buckling temperature of a rectangular PP-modified concrete panel at 10% volumetric pumice content, as a function of the length-to-thickness ratio (a/h_w) for aspect ratios $a/b = 1$ and $a/b = \sqrt{2}$

The results indicate that increasing PP content leads to a systematic increase in the critical thermal buckling temperature, particularly for panels with moderate slenderness ratios. This behavior is consistent with the reduced thermal expansion and modified stiffness resulting from PP incorporation, which together influence the thermo-elastic stability response. However, panels with higher aspect ratios remain more sensitive to thermal instability, confirming the dominant role of geometric slenderness in buckling behavior. These findings highlight the coupled influence of material modification and geometry within the framework of the present analytical model, while further experimental or numerical validation would be required to generalize the conclusions to practical structural applications.

Based on the computed data, the sensitivity of the critical thermal buckling temperature (ΔT_{cr}) to variations in the effective thermal expansion coefficient (α_{hom}) can be quantified for each wall slenderness (a/h_w). It can be seen from Table 10, for a 10% PP inclusion, where α_{hom} decreases by ~6.3% compared to pure concrete, the relative change in ΔT_{cr} ranges from 16% to 16.7% across all a/hw ratios. This corresponds to a sensitivity coefficient $S_{\alpha}^{\Delta T_{cr}} = [\Delta(\Delta Tcr)/\Delta T_{cr0}]/(\Delta\alpha/\alpha) \approx 2.54 - 2.69$, indicating that ΔT_{cr} increases moderately as α_{hom} decreases.

Table 10. Sensitivity of the critical thermal buckling temperature (ΔT_{cr}) of a square PP-modified concrete panel to reductions in the effective thermal expansion coefficient (α_{hom}) for varying wall slenderness ratios (a/h_w)

Wall slenderness (a/h_w)	ΔT_{cr} (0% PP) $\times 10^2$ °C	ΔT_{cr} (10% PP) $\times 10^2$ °C	$\Delta(\Delta T_{cr})$ (%)	$\Delta\alpha_{hom}$ (%)	Sensitivity $S_{\alpha}^{\Delta T_{cr}}$
5	39.78	46.14	16.0	-6.3	2.54
10	11.34	13.23	16.7	-6.3	2.65
15	5.18	6.05	16.8	-6.3	2.67
20	2.94	3.44	16.9	-6.3	2.68
25	1.89	2.21	17.0	-6.3	2.70
30	1.31	1.54	16.9	-6.3	2.69
35	0.97	1.13	16.9	-6.3	2.68
40	0.74	0.87	16.9	-6.3	2.68
45	0.59	0.69	16.9	-6.3	2.69
50	0.48	0.56	16.9	-6.3	2.69

$\Delta(\Delta T_{cr})$ (%): Relative increase in critical thermal buckling temperature from 0% to 10% PP.

$\Delta\alpha_{hom}$ (%): Reduction in thermal expansion coefficient due to 10% PP.

The reduction in α_{hom} due to the low thermal expansion of PP reduces the thermal in-plane forces ($N_T \propto E \times \alpha \times \Delta T$) that drive thermal buckling. Consequently, the critical temperature rises, especially for moderately slender walls. Thinner or more slender walls still remain more prone to thermal instability, but the inclusion of PP consistently shifts the buckling threshold upward. This quantitative assessment provides a clearer link between microstructural modification (PP incorporation) and the panel's thermo-mechanical stability.

5. Conclusions

This study presented an analytical framework to evaluate the coupled mechanical and thermal response of pumice powder PP–modified concrete walls using a combined Reuss–Voigt–Luo homogenization scheme and refined plate theory. The model successfully captured the influence of PP on stiffness, heat transfer, and thermal buckling behavior. The main findings can be summarized as follows:

- In accordance with experimental studies, our analytical modelling show that PP addition (2.5–10%) slightly decreases the elastic modulus and critical mechanical buckling load, due to the lower stiffness of pumice.
- Effective thermal conductivity decreases by up to ≈8–9%, enhancing insulation performance.
- The thermal resistance increases by 18–20% with 10% PP, regardless of wall thickness.
- The thermal transmittance value decreases by ≈17%, limiting heat transfer under summer and winter loading conditions.
- PP reduces heat ingress in hot climates and heat loss in cold climates across all thicknesses.
- The critical thermal buckling temperature increases with PP content, indicating better resistance to temperature-induced instability.
- The homogenization model shows good agreement with experimental data for elastic modulus, thermal conductivity, and thermal expansion.

These results demonstrate that pumice powder offers a balanced combination of enhanced thermal insulation and acceptable structural stability, confirming its suitability for sustainable and energy-efficient concrete wall systems.

This work provides one of the first analytical models capable of predicting the combined mechanical, thermal, and thermo-mechanical buckling behavior of PP-modified concrete walls. The approach links microstructural material behavior to structural-scale performance and offers a predictive framework for thermo-mechanical assessment. However, several simplifying assumptions affect the model's accuracy. The homogenization strategy assumes a homogeneous and isotropic composite, which may slightly overestimate stiffness and critical buckling loads by neglecting local heterogeneity and directional porosity effects. The adoption of linear thermo-elastic behavior and idealized simply supported boundary conditions may further limit applicability under nonlinear response or realistic restraint conditions. Additionally, moisture transport, temperature dependency of material properties, aging, and interfacial transition zone effects were neglected; these factors could alter thermal conductivity and expansion coefficients, potentially leading to non-conservative predictions under long-term or severe thermal gradients. The analysis was restricted to PP contents up to 10%, and higher inclusion levels may introduce nonlinear interaction effects beyond the validity of the present formulation. These aspects define the current validity domain and motivate future multi-physics and experimentally validated extensions.

Future research should therefore incorporate nonlinear and post-buckling effects, include realistic microstructural characterizations obtained from SEM or micro-CT imaging, and examine the influence of long-term factors such as creep, cracking, moisture transport, fire exposure, and interfacial transition zone (ITZ) effects. Among these aspects, the incorporation of material nonlinearity and post-buckling behavior is the most urgent, as the present linear thermo-elastic assumption has the strongest influence on the accuracy of critical buckling predictions near instability. While the current study uses single, fixed values for the elastic modulus, thermal conductivity, and thermal expansion coefficient of pumice, these values are supported by published references, which also adopt fixed parameters for similar analyses. However, sensitivity results indicate that stiffness-related parameters exert the largest impact on predicted buckling loads, suggesting that future efforts should first refine their experimental calibration. Experimental testing on large-scale PP-reinforced concrete walls is needed to validate thermal buckling behavior and quantify real-world energy savings. Such validation is particularly important to assess the effect of the homogeneity assumption, which may lead to slight overestimation of structural stiffness at higher PP contents. Additionally, hybrid mixtures combining PP with fibers, nano-additives, or recycled materials, as well as optimization studies for different climate zones, offer promising directions to further enhance the structural and thermal performance of eco-efficient concrete.

Appendix A

The stress resultants of the PP-modified concrete panel are derived by substituting the displacement field (Eq. 21) into the constitutive relations (Eq. 23). The resulting expressions relate the bending and in-plane stress resultants to the material stiffness parameters and displacement components, can be expressed as follows:

$$\begin{Bmatrix} N_x \\ N_y \\ N_{xy} \end{Bmatrix} = A_{ij} \begin{Bmatrix} \dfrac{\partial u_x}{\partial x} \\ \dfrac{\partial u_y}{\partial y} \\ \left(\dfrac{\partial u_x}{\partial y} + \dfrac{\partial u_y}{\partial x}\right) \end{Bmatrix} + B_{ij} \begin{Bmatrix} \dfrac{-\partial^2 w_b}{\partial x^2} \\ \dfrac{\partial^2 w_b}{\partial y^2} \\ -2\dfrac{\partial^2 w_b}{\partial x \partial y} \end{Bmatrix} + B_{ij}^s \begin{Bmatrix} \dfrac{-\partial^2 w_s}{\partial \alpha^2} \\ \dfrac{\partial^2 w_s}{\partial y^2} \\ -2\dfrac{\partial^2 w_b}{\partial x \partial y} \end{Bmatrix} - \begin{Bmatrix} N_{Tx} \\ N_{Ty} \\ N_{Txy} \end{Bmatrix}$$

$$\begin{Bmatrix} M_x^b \\ M_y^b \\ M_{xy}^b \end{Bmatrix} = B_{ij} \begin{Bmatrix} \dfrac{\partial u_x}{\partial x} \\ \dfrac{\partial u_y}{\partial y} \\ \left(\dfrac{\partial u_x}{\partial y} + \dfrac{\partial u_y}{\partial x}\right) \end{Bmatrix} + D_{ij} \begin{Bmatrix} \dfrac{-\partial^2 w_b}{\partial x^2} \\ \dfrac{\partial^2 w_b}{\partial y^2} \\ -2\dfrac{\partial^2 w_b}{\partial x \partial y} \end{Bmatrix} + D_{ij}^s \begin{Bmatrix} \dfrac{-\partial^2 w_s}{\partial \alpha^2} \\ \dfrac{\partial^2 w_s}{\partial y^2} \\ -2\dfrac{\partial^2 w_b}{\partial x \partial y} \end{Bmatrix} - \begin{Bmatrix} M_{Tx}^b \\ M_{Ty}^b \\ M_{Txy}^b \end{Bmatrix}$$

$$\begin{Bmatrix} M_x^s \\ M_y^s \\ M_{xy}^s \end{Bmatrix} = B_{ij}^s \begin{Bmatrix} \dfrac{\partial u_x}{\partial x} \\ \dfrac{\partial u_y}{\partial y} \\ \left(\dfrac{\partial u_x}{\partial y} + \dfrac{\partial u_y}{\partial x}\right) \end{Bmatrix} + D_{ij}^s \begin{Bmatrix} \dfrac{-\partial^2 w_b}{\partial x^2} \\ \dfrac{\partial^2 w_b}{\partial y^2} \\ -2\dfrac{\partial^2 w_b}{\partial x \partial y} \end{Bmatrix} + H_{ij}^s \begin{Bmatrix} \dfrac{-\partial^2 w_s}{\partial \alpha^2} \\ \dfrac{\partial^2 w_s}{\partial y^2} \\ -2\dfrac{\partial^2 w_b}{\partial x \partial y} \end{Bmatrix} - \begin{Bmatrix} M_{Tx}^s \\ M_{Ty}^s \\ M_{Txy}^s \end{Bmatrix}$$

$$\begin{Bmatrix} Q_{xz} \\ Q_{yz} \end{Bmatrix} = A_{ij}^s \begin{Bmatrix} \dfrac{\partial w_s}{\partial x} \\ \dfrac{\partial w_s}{\partial y} \end{Bmatrix}$$

In these expressions, A_{ij}, B_{ij}, D_{ij}, B_{ij}^s, D_{ij}^s, H_{ij}^s, and A_{ij}^s represent the plate stiffness coefficients. These constants characterize the in-plane, bending, and shear stiffness of the PP-modified concrete panel and are defined through the integration of the homogenized elastic properties across the wall's thickness, reflecting the combined influence of the concrete matrix and PP inclusions.

$$A_{ij} = b\int_{-h_w/2}^{h_w/2} \tilde{Q}_{ij}\, dz; B_{ij} = b\int_{-h_w/2}^{h_w/2} z\tilde{Q}_{ij}\, dz; D_{ij} = b\int_{-h_w/2}^{h_w/2} z^2\tilde{Q}_{ij}\, dz;$$

$$B_{ij}^s = b\int_{\frac{-h_w}{2}}^{\frac{h_w}{2}} f(z)\tilde{Q}_{ij}\, dz; D_{ij}^s = b\int_{\frac{-h_w}{2}}^{\frac{h_w}{2}} zf(z)\tilde{Q}_{ij}\, dz; H_{ij}^s = b\int_{\frac{-h_w}{2}}^{\frac{h_w}{2}} f(z)^2\tilde{Q}_{ij}\, dz;$$

$$A_{ij}^s = b\int_{\frac{-h_w}{2}}^{\frac{h_w}{2}} g(z)^2\tilde{Q}_{ij}\, dz;$$

References

[1] Zhai, P., et al. Global Warming of 1.5° C. An IPCC Special Report on the impacts of global warming of 1.5° C above pre-industrial levels and related global greenhouse gas emission pathways, in the context of strengthening the global response to the threat of climate change. Sustainable development, and efforts to eradicate poverty, 2018; 32.

[2] Huseien, G.F., N.H.A. Khalid, and J. Mirza. Nanotechnology for Smart Concrete, CRC Press, Boca Raton, 2022.

[3] Modi, P.I. and C.N. Patel. Repair and Rehabilitation of Concrete Structures, PHI Learning Pvt. Ltd., 2015.

[4] Mosley, W.H., J.H. Bungey, and R. Hulse. Reinforced concrete design, Springer, 1999.

[5] Carlsen, L. and R. Bruggemann. The 17 United Nations' sustainable development goals: a status by 2020. International Journal of Sustainable Development & World Ecology, 2022; 29(3): 219-229. https://doi.org/10.1080/13504509.2021.1948456

[6] Association, G.C.a.C. The GCCA 2050 Cement and Concrete Industry Roadmap for Net Zero Concrete. 2020. https://gccassociation.org/concretefuture/wp-content/uploads/2022/10/GCCA-Concrete-Future-RoadmapDocument-AW-2022.pdf.(2020)

[7] Woodson, R.D. Concrete structures: protection, repair and rehabilitation, Butterworth-Heinemann, 2009.

[8] Wight, J.K. and J.G. MacGregor. Reinforced concrete, Pearson Education UK Sydney, NSW, 2016.

[9] Alexander, M., A. Bentur, and S. Mindess. Durability of concrete: design and construction, CRC Press, 2017.

[10] Yusra, A., et al. Optimizing concrete strength through pozzolan variation, heat treatment, and alkaline solution modulation: A comprehensive study. Res. Eng. Struct. Mater., 2025; 11(1): 97-111. http://dx.doi.org/10.17515/resm2024.175ma0205rs

[11] Aïtcin, P.-C. Binders for durable and sustainable concrete, CRC Press, 2007.

[12] Chatbi, M., et al. Computational Models for the Vibration and Modal Analysis of Silica Nanoparticle-Reinforced Concrete Slabs with Elastic and Viscoelastic Foundation Effects. Modelling, 2026. **7**, 8 http://dx.doi.org/10.3390/modelling7010008

[13] Asmara, Y.P. Concrete Reinforcement Degradation and Rehabilitation: Damages, Corrosion and Prevention, Springer Nature, 2023.

[14] Hassoun, M.N. and A. Al-Manaseer. Structural concrete: theory and design, John wiley & sons, 2020.

[15] Gopalakrishnan, K., et al. Nanotechnology in Civil Infrastructure, Springer, Berlin, Heidelberg, 273, 2011.

[16] Pacheco-Torgal, F., Introduction to nanotechnology in eco-efficient construction, in Nanotechnology in Eco-Efficient Construction. 2013, Elsevier. p. 1-6.

[17] Djeddou, M., et al. Development of eco-friendly self-compacting concrete using marble powder, blast furnace slag and glass fibre-reinforced plastic waste: Application of mixture design approach. Eng. Struct. Mater., 2025; 11(1). http://dx.doi.org/10.17515/resm2024.178ma0208rs

[18] Thirupathi, S., S. Palanisamy, and V. Asokan. Enhancing sustainability in construction: Exploring the self-healing mechanisms of bio-concrete. Res. Eng. Struct. Mater., 2025; 11(6): 2731–2744. http://dx.doi.org/10.17515/resm2025-517ma1105rs
[19] Harrat, Z.R., et al. On the static behavior of nano Si02 based concrete beams resting on an elastic foundation. Computers and Concrete, 2021; 27(6): 575. https://doi.org/10.12989/cac.2021.27.6.575
[20] Chatbi, M., et al. Bending analysis of nano-SiO2 reinforced concrete slabs resting on elastic foundation. Structural Engineering and Mechanics, An Int'l Journal, 2022; 84(5): 685-697. https://doi.org/10.12989/sem.2022.84.5.685
[21] Dine Elhennani, S., et al. Buckling and Free Vibration Analyses of Various Nanoparticle Reinforced Concrete Beams Resting on Multi-Parameter Elastic Foundations. Materials, 2023. **16**, DOI: https://doi.org/10.3390/ma16175865.
[22] Kecir, A., et al. Enhancing the Mechanical Performance of Concrete Slabs through the Incorporation of Nano-sized Iron Oxide Particles (Fe2O3): Non-local Bending Analysis. Periodica Polytechnica Civil Engineering, 2024; 68(3): 842-858. https://doi.org/10.3311/PPci.23016
[23] Harrat, Z.R., et al. Bending analysis of nano-Fe2</sub>O₃ reinforced concrete slabs exposed to temperature fields and supported by viscoelastic foundation. Advances in concrete construction, 2024: 111-126. https://doi.org/10.12989/acc.2024.17.2.111
[24] Harrat, Z.R., et al. Modeling the Thermoelastic Bending of Ferric Oxide (Fe2O3) Nanoparticles-Enhanced RC Slabs. Materials, 2023; 16(8): 3043. https://doi.org/10.3390/ma16083043
[25] Benfrid, A., et al. Selective Integration of Waste-Derived Glass Nanopowders in Structural Wall Concrete: Improving Thermal Efficiency and Elasto-Mechanical Properties for Sustainable Construction. Periodica Polytechnica Civil Engineering, 2025; 69(3): 954-965. https://doi.org/10.3311/PPci.39913
[26] Cavaleri, L., N. Miraglia, and M. Papia. Pumice concrete for structural wall panels. Engineering Structures, 2003; 25(1): 115-125. https://doi.org/10.1016/S0141-0296(02)00123-2
[27] Granata, M.F. Pumice powder as filler of self-compacting concrete. Construction and Building Materials, 2015; 96: 581-590. https://doi.org/10.1016/j.conbuildmat.2015.08.040
[28] Kurt, M., et al. The effect of pumice powder on the self-compactability of pumice aggregate lightweight concrete. Construction and Building Materials, 2016; 103: 36-46. https://doi.org/10.1016/j.conbuildmat.2015.11.043
[29] Zeyad, A.M. and A. Almalki. Role of particle size of natural pozzolanic materials of volcanic pumice: flow properties, strength, and permeability. Arabian Journal of Geosciences, 2021; 14(2): 107. https://doi.org/10.1007/s12517-020-06443-y
[30] Zeyad, A.M., et al. Production of geopolymer concrete by utilizing volcanic pumice dust. Case Studies in Construction Materials, 2022; 16: e00802. https://doi.org/10.1016/j.cscm.2021.e00802
[31] Zeyad, A.M., M. Shubaili, and A. Abutaleb. Using volcanic pumice dust to produce high-strength self-curing concrete in hot weather regions. Case Studies in Construction Materials, 2023; 18: e01927. https://doi.org/10.1016/j.cscm.2023.e01927
[32] Hossain, K.M.A. Blended cement using volcanic ash and pumice. Cement and Concrete Research, 2003; 33(10): 1601-1605. https://doi.org/10.1016/S0008-8846(03)00127-3
[33] Karthika, R.B., et al. Experimental study on lightweight concrete using pumice aggregate. Materials Today: Proceedings, 2021; 43: 1606-1613. https://doi.org/10.1016/j.matpr.2020.09.762
[34] Moolchandani, K. Advancements in pumice-based concrete: A comprehensive review. Next Materials, 2025; 8: 100646. https://doi.org/10.1016/j.nxmate.2025.100646
[35] Ghanim, A.A.J., et al. Experimental investigation of industrial wastes in concrete: Mechanical and microstructural evaluation of pumice powder and Fly Ash in concrete. Case Studies in Construction Materials, 2023; 18: e01999. https://doi.org/10.1016/j.cscm.2023.e01999
[36] Amenu, T., A. Geremew, and H. Ayene. A Study on The Suitability of Pumice Stone Powder As A Cementitious Material in Sustainable Green Concrete Production. International Journal of Sustainable Construction Engineering and Technology, 2023; 14(4): 64-78.
[37] Hashim, A.A. and H.M. Owaid. A Review of Workability and Mechanical Behavior of Self-Compacting Construction Composites Incorporating Nanomaterials. Journal of University of Babylon for Engineering Sciences, 2024; 32(5): 119 - 131. https://doi.org/10.29196/5sjfe077
[38] Rathee, M. and A. Misra. Performance of alkali-activated aluminosilicate geopolymer mortar under exposure to acid, sulfate and high temperature. Magazine of Concrete Research, 2025; 77(3-4): 209-227. https://doi.org/10.1680/jmacr.24.00058
[39] Ma, H., et al. Mechanical properties and microstructural characteristics of coral-aggregate-concrete ITZ: Experimental study. Journal of Building Engineering, 2023; 72: 106647. https://doi.org/10.1016/j.jobe.2023.106647
[40] Rath, B., et al. An innovative technique for internal curing of concrete with brick aggregate, nanoparticles of Al2O3 and rubber latex. Innovative Infrastructure Solutions, 2021; 7(1): 77. https://doi.org/10.1007/s41062-021-00673-z

[41] Ali, H.K., S.R. Abid, and N. Tayşi Thermal Behaviour and Microstructure of Self-Cured High-Strength Plain and Fibrous Geopolymer Concrete Exposed to Various Fire Scenarios. Buildings, 2023. **13**, 2444 DOI: https://doi.org/10.3390/buildings13102444.
[42] Zhao, H., et al. Numerical insights into the effect of ITZ and aggregate strength on concrete properties. Theoretical and Applied Fracture Mechanics, 2022; 120: 103415. https://doi.org/10.1016/j.tafmec.2022.103415
[43] Li, X., et al. Investigation on Microstructure, Composition, and Cytocompatibility of Natural Pumice for Potential Biomedical Application. Tissue Engineering Part C: Methods, 2009; 16(3): 427-434. https://doi.org/10.1089/ten.tec.2009.0285
[44] Shi, L., et al. Petrochemistry of pumices of various colors produced by the eruption of Changbaishan Tianchi volcano at 1000 years ago. Seismol Geol, 2005; 27(1): 73-82.
[45] Turhan, Ş. and L. Gündüz. Determination of specific activity of 226Ra, 232Th and 40K for assessment of radiation hazards from Turkish pumice samples. Journal of Environmental Radioactivity, 2008; 99(2): 332-342. https://doi.org/10.1016/j.jenvrad.2007.08.022
[46] Liu, K., et al. Effects of Pumice-Based Porous Material on Hydration Characteristics and Persistent Shrinkage of Ultra-High Performance Concrete (UHPC). Materials, 2019. **12**, 11 DOI: https://doi.org/10.3390/ma12010011.
[47] Tapan, M., et al. Effect of physical, chemical and electro-kinetic properties of pumice on strength development of pumice blended cements. Materials and Structures, 2013; 46(10): 1695-1706. https://doi.org/10.1617/s11527-012-0008-y
[48] Rashad, A.M. An Overview of Pumice Stone as a Cementitious Material – the Best Manual for Civil Engineer. Silicon, 2021; 13(2): 551-572. https://doi.org/10.1007/s12633-020-00469-3
[49] Adil Rasool, D., H. Al-Moameri, and M. Abdulkarem. Review Of Recycling Natural And Industrial Materials Employments In Concrete. Journal of Engineering and Sustainable Development, 2023; 27(2): 180-195. https://doi.org/10.31272/jeasd.27.2.3
[50] Tahwia, A.M., et al. Valorization of recycled concrete powder, clay brick powder, and volcanic pumice powder in sustainable geopolymer concrete. Scientific Reports, 2025; 15(1): 11049. https://doi.org/10.1038/s41598-025-93598-x
[51] Tran, Q. and P. Ghosh. Influence of pumice on mechanical properties and durability of high performance concrete. Construction and Building Materials, 2020; 249: 118741. https://doi.org/10.1016/j.conbuildmat.2020.118741
[52] Abraham, A.L. and R.P. Mohan. Study on Strength Properties of Concrete using Pumice Powder Pozzolan and Polypropylene Fibers. IOP Conference Series: Materials Science and Engineering, 2020; 936(1): 012002. https://doi.org/10.1088/1757-899X/936/1/012002
[53] Waqar, A., et al. Effect of volcanic pumice powder ash on the properties of cement concrete using response surface methodology. Journal of Building Pathology and Rehabilitation, 2023; 8(1): 17. https://doi.org/10.1007/s41024-023-00265-7
[54] López-Gonzalez, P.J., et al. Impact of Pumice Substitution on Mortar Properties: A Case Study on Mechanical Performance and XRD Analysis. Infrastructures, 2025. 10, 95 https://doi.org/10.3390/infrastructures10040095
[55] Kirchhoff, G. Über das Gleichgewicht und die Bewegung einer elastischen Scheibe. 1850; 1850(40): 51-88. https://doi.org/10.1515/crll.1850.40.51
[56] Whitney, J.M. Shear Correction Factors for Orthotropic Laminates Under Static Load. Journal of Applied Mechanics, 1973; 40(1): 302-304. https://doi.org/10.1115/1.3422950
[57] Reddy, J.N. A Simple Higher-Order Theory for Laminated Composite Plates. Journal of Applied Mechanics, 1984; 51(4): 745-752. https://doi.org/10.1115/1.3167719
[58] Touratier, M. An efficient standard plate theory. International Journal of Engineering Science, 1991; 29(8): 901-916. https://doi.org/10.1016/0020-7225(91)90165-Y
[59] Karama, M., M. Touratier, and A. Idlbi. An evaluation of the edge solution for a higher-order laminated plate theory. Composite Structures, 1993; 25(1-4): 495-502.
[60] Lee, Y.Y., X. Zhao, and K.M. Liew. Thermoelastic analysis of functionally graded plates using the element-free kp-Ritz method. Smart Materials and Structures, 2009; 18(3): 035007. https://doi.org/10.1088/0964-1726/18/3/035007
[61] Sun, Y., S.-R. Li, and R.C. Batra. Thermal buckling and post-buckling of FGM Timoshenko beams on nonlinear elastic foundation. Journal of Thermal Stresses, 2016; 39(1): 11-26. https://doi.org/10.1080/01495739.2015.1120627
[62] Prakash, T. and M. Ganapathi. Asymmetric flexural vibration and thermoelastic stability of FGM circular plates using finite element method. Composites Part B: Engineering, 2006; 37(7): 642-649. https://doi.org/10.1016/j.compositesb.2006.03.005
[63] Zenkour, A.M. and M. Sobhy. Thermal buckling of various types of FGM sandwich plates. Composite Structures, 2010; 93(1): 93-102. https://doi.org/10.1016/j.compstruct.2010.06.012

[64] Yang, J., et al. Thermo-mechanical post-buckling of FGM cylindrical panels with temperature-dependent properties. International Journal of Solids and Structures, 2006; 43(2): 307-324. https://doi.org/10.1016/j.ijsolstr.2005.04.001
[65] Niknam, H. and A.H. Akbarzadeh. Thermo-mechanical bending of architected functionally graded cellular beams. Composites Part B: Engineering, 2019; 174: 107060. https://doi.org/10.1016/j.compositesb.2019.107060
[66] Mallios, D.A., E.E. Theotokoglou, and C.C. Koutsoumaris. Thermomechanical analysis of FGM sandwich beams through graded FEM. Journal of Thermal Stresses: 1-19. https://doi.org/10.1080/01495739.2025.2548557
[67] Sayyad, A.S. and Y.M. Ghugal. Modeling and analysis of functionally graded sandwich beams: a review. Mechanics of Advanced Materials and Structures, 2019; 26(21): 1776-1795. https://doi.org/10.1080/15376494.2018.1447178
[68] Sayyad, A.S. and Y.M. Ghugal. Bending, buckling and free vibration of laminated composite and sandwich beams: A critical review of literature. Composite Structures, 2017; 171: 486-504. https://doi.org/10.1016/j.compstruct.2017.03.053
[69] Sayyad, A.S. and Y.M. Ghugal. On the free vibration analysis of laminated composite and sandwich plates: A review of recent literature with some numerical results. Composite Structures, 2015; 129: 177-201. https://doi.org/10.1016/j.compstruct.2015.04.007
[70] Sayyad, A.S. and Y.M. Ghugal. Single variable refined beam theories for the bending, buckling and free vibration of homogenous beams. Applied and Computational Mechanics, 2016; 10(2).
[71] Sayyad, A.S. and Y.M. Ghugal. Assessment of refined higher order theories for the static and vibration analysis of laminated composite cylindrical shells. Journal of Mechanical Engineering and Sciences, 2022; 16(2): 8848 - 8861. https://doi.org/10.15282/jmes.16.2.2022.04.0700
[72] Shimpi, R.P. Refined Plate Theory and Its Variants. AIAA Journal, 2002; 40(1): 137-146. https://doi.org/10.2514/2.1622
[73] Chitour, M., et al. Stability analysis of imperfect FG sandwich plates containing metallic foam cores under various boundary conditions. Structures, 2024; 61: 106021. https://doi.org/10.1016/j.istruc.2024.106021
[74] Voigt, W. Lehrbuch der kristallphysik:(mit ausschluss der kristalloptik), BG Teubner, Vol. 34, 1910.
[75] Reuss, A. Berechnung der Fließgrenze von Mischkristallen auf Grund der Plastizitätsbedingung für Einkristalle. ZAMM - Journal of Applied Mathematics and Mechanics / Zeitschrift für Angewandte Mathematik und Mechanik, 1929; 9(1): 49-58. https://doi.org/10.1002/zamm.19290090104
[76] Jayadurgalakshmi, M. and S. Kandasamy. Behaviour of cenosphere and pumice powder as partial cement substitute material in the sustainable production of concrete. Journal of Building Pathology and Rehabilitation, 2024; 9(1): 47. https://doi.org/10.1007/s41024-024-00397-4
[77] Bakis, A., et al. Mechanical Properties of Reactive Powder Concretes Produced Using Pumice Powder. Journal of Wuhan University of Technology-Mater. Sci. Ed., 2019; 34(2): 353-360. https://doi.org/10.1007/s11595-019-2059-1
[78] Kabay, N., N. Miyan, and H. Özkan. Utilization of pumice powder and glass microspheres in cement mortar using paste replacement methodology. Construction and Building Materials, 2021; 282: 122691. https://doi.org/10.1016/j.conbuildmat.2021.122691
[79] Blanc, X., C. Le Bris, and P.L. Lions. Stochastic homogenization and random lattices. Journal de Mathématiques Pures et Appliquées, 2007; 88(1): 34-63. https://doi.org/10.1016/j.matpur.2007.04.006
[80] Charalambakis, N. Homogenization Techniques and Micromechanics. A Survey and Perspectives. Applied Mechanics Reviews, 2010; 63(3). https://doi.org/10.1115/1.4001911
[81] Trovalusci, P., et al. Scale-dependent homogenization of random composites as micropolar continua. European Journal of Mechanics - A/Solids, 2015; 49: 396-407. https://doi.org/10.1016/j.euromechsol.2014.08.010
[82] Wang, W., et al. Effect of cement matrix on mechanical properties of cemented granular materials. Powder Technology, 2019; 350: 107-116. https://doi.org/10.1016/j.powtec.2019.03.040
[83] Khazma, M., et al. Optimization of flax shive-cementitious composites: Impact of different aggregate treatments using linseed oil. Industrial Crops and Products, 2014; 61: 442-452. https://doi.org/10.1016/j.indcrop.2014.07.041
[84] Luo, Y. Improved Voigt and Reuss Formulas with the Poisson Effect. Materials, 2022. **15**, 5656 DOI: https://doi.org/10.3390/ma15165656
[85] Eucken, A. Allgemeine Gesetzmäßigkeiten für das Wärmeleitvermögen verschiedener Stoffarten und Aggregatzustände. Forschung auf dem Gebiet des Ingenieurwesens A, 1940; 11(1): 6-20. https://doi.org/10.1007/BF02584103
[86] Neville, A.M. and J.J. Brooks. Concrete technology, Longman Scientific & Technical England, Vol. 438, 1987.

[87] Bilir, T. Pomza Agregali Betonlarin Elastisite Modüllerinin Tahmininde Bazi Ampirik Ve Kompozit Modellerin Performanslarinin İncelenmesi. Niğde Ömer Halisdemir Üniversitesi Mühendislik Bilimleri Dergisi, 2016; 5(2): 195-207. https://doi.org/10.28948/ngumuh.295581
[88] Kalkan, Ş.O. and L. Gündüz. Use of pumice aggregate in cementitious rheoplastic lightweight concrete. Journal of Sustainable Construction Materials and Technologies, 2023; 8(1): 57-65. https://doi.org/10.47481/jscmt.1214086
[89] Européen, C. Eurocode 2: Design of concrete structures—Part 1-1: General rules and rules for buildings. London: British Standard Institution, 2004: 37.